Geoscience Frontiers 12 (2021) 101247

HOSTED BY

ELSEVIER

Contents lists available at ScienceDirect

Geoscience Frontiers

journal homepage: www.elsevier.com/locate/gsf

Research Paper

Timing of Proterozoic magmatism in the Sunsas belt, Bolivian Precambrian Shield, SW Amazonian Craton

Ingrid M. Nedel [a,*], Reinhardt A. Fuck [a], Amarildo S. Ruiz [b], Gerardo R. Matos-Salinas [c], Alanielson da C.D. Ferreira [d]

[a] *Instituto de Geociências, Universidade de Brasília (UnB), Brasília-DF, Brazil*
[b] *Faculdade de Geociências, Universidade Federal de Mato Grosso, Cuiabá-MT, Brazil*
[c] *Instituto de Investigaciones Geológicas y del Medio Ambiente, Universidad Mayor de San Andrés (UMSA), Pabellón Geología, Calle 27, Campus Universitario Cota Cota, La Paz, Bolivia*
[d] *Department of Earth Sciences, Stellenbosch University, Private Bag X1, Matieland, 7602 Stellenbosch, South Africa*

ARTICLE INFO

Article history:
Received 2 November 2020
Revised 25 May 2021
Accepted 3 June 2021
Available online 5 June 2021
Handling Editor: K. Szilas

Keywords:
SW Amazonian Craton
Sunsas belt
U–Pb geochronology
Zircon
Monazite

ABSTRACT

We present new U–Pb zircon and monazite ages from the Sunsas belt granitic magmatism in Bolivia, SW Amazonian Craton. The geochronological results revealed four major magmatic events recorded along the Sunsas belt domains. The older igneous event formed a granitic basement coeval to the Rio Apa Terrane (1.95 – 1.85 Ga) in the southern domain. The second magmatic episode is represented by 1.68 Ga granites associated to the Paraguá Terrane (1.69–1.66 Ga) in the northern domain. The 1.37–1.34 Ga granites related to San Ignacio orogeny represent the third and more pervasive magmatic event, recorded throughout the Sunsas belt. Moreover, magmatic ages of ~1.42 Ga revealed that the granitogenesis associated to the Santa Helena orogeny also affected the Sunsas belt, indicating that it was not restricted to the Jauru Terrane. Lastly, the 1.10–1.04 Ga youngest magmatism was developed during the Sunsas orogeny and represents the final magmatic evolution related to Rodinia assembly. Likewise, the 1.95–1.85 and 1.68 Ga inherited zircon cores obtained in the ~1.3 Ga and 1.0 Ga granite samples suggest strong partial melting of the Paleoproterozoic sources. The 1079 ± 14 Ma and 1018 ± 6 Ma monazite crystallization ages can be correlated to the collisional tectono-thermal event of the Sunsas orogeny, associated to reactions of medium- to high-grade metamorphism. Thus, the Sunsas belt was built by heterogeneous 1.95–1.85 Ga and 1.68 Ga crustal fragments that were reworked at 1.37–1.34 Ga and 1.10–1.04 Ga related to orogenic collages. Furthermore, the 1.01 Ga monazite age suggests that granites previously dated by zircon can bear evidence of a younger thermal history. Therefore, the geochronological evolution of the Sunsas belt may have been more complex than previously thought.

1. Introduction

The Proterozoic eon represents the most significant time for continental growth produced by magmatic arcs and successive terrane accretions (e.g., Cawood et al., 2013; Holder et al., 2019; Ferreira et al., 2020). This time interval included strong reworking processes during episodic supercontinent assembly and breakup processes (1.7–1.3 Ga and 1.1–0.7 Ga) (e.g., Condie, 2004; Hawkesworth et al., 2010; Nance et al., 2014; Ernst et al., 2016). The Rodinia supercontinent assembly is a significant stage for the global Proterozoic evolution (e.g., Meert, 2001; Li et al., 2008; Nance et al., 2014). It marks the amalgamation of Archean to early Proterozoic continental fragments during late Mesoproterozoic to Neoproterozoic times, leading to maximum crustal thickness and magmatism during the Grenville-age collage (e.g., Meert, 2001; Li et al., 2008; Nance et al., 2014). The magmatism associated with Rodinia formation shows diachronic episodes and presents a wide spatial distribution. For instance, it is recorded in the eastern margin of Laurentia, southwestern portion of the Amazonian Craton, western margin of Baltica, Southern China Craton, Australia (North Queensland) and eastern margin of Antarctica (e.g., King Island-Transantarctic Mountains; McLelland et al., 1996; Fitzsimons, 2000; Li et al., 2002; Keppie et al., 2003; Hodych et al., 2004; Fioretti et al., 2005; Bingen et al., 2021).

In the SW Amazonian Craton, the Sunsas Province represents the final Proterozoic continental accretion with tectonic implications for reconstructions of the Rodinia assembly (e.g., Sadowski

* Corresponding author.
E-mail address: ingrid_mn@hotmail.com (I.M. Nedel).

https://doi.org/10.1016/j.gsf.2021.101247
1674-9871/

and Bettencourt, 1996; Tohver et al., 2002, 2006; Loewy et al., 2004; Boger et al., 2005; Fuck et al., 2008; Li et al., 2008; Teixeira et al., 2010). The Sunsas belt is the southwestern tectonic component of the Sunsas Province, evolved from an oblique collision characterized by sinistral shear zones at 1.1–1.0 Ga during the Sunsas orogeny (e.g., Boger et al., 2005; Teixeira et al., 2010). In addition, the granitic magmatism related to the Sunsas orogeny presents heterogeneous Archaean and Paleoproterozoic sources (Nedel et al., 2020). In this context, we present U–Pb zircon and monazite ages of magmatic rocks exposed in the Sunsas belt – Bolivia. These unpublished results aim to (1) explore magmatic episodes recorded in the Precambrian Sunsas belt; (2) apply U–Pb monazite dating to recognize metamorphic and late thermal activities related to the Sunsas orogeny; (3) define the Sunsas belt magmatic sources; (4) compare the Bolivian basement evolution with the Rio Apa terrane.

2. Geological setting

In the northern of South America, the Amazonian Craton represents continent-scale terrain accretion processes from Archean to

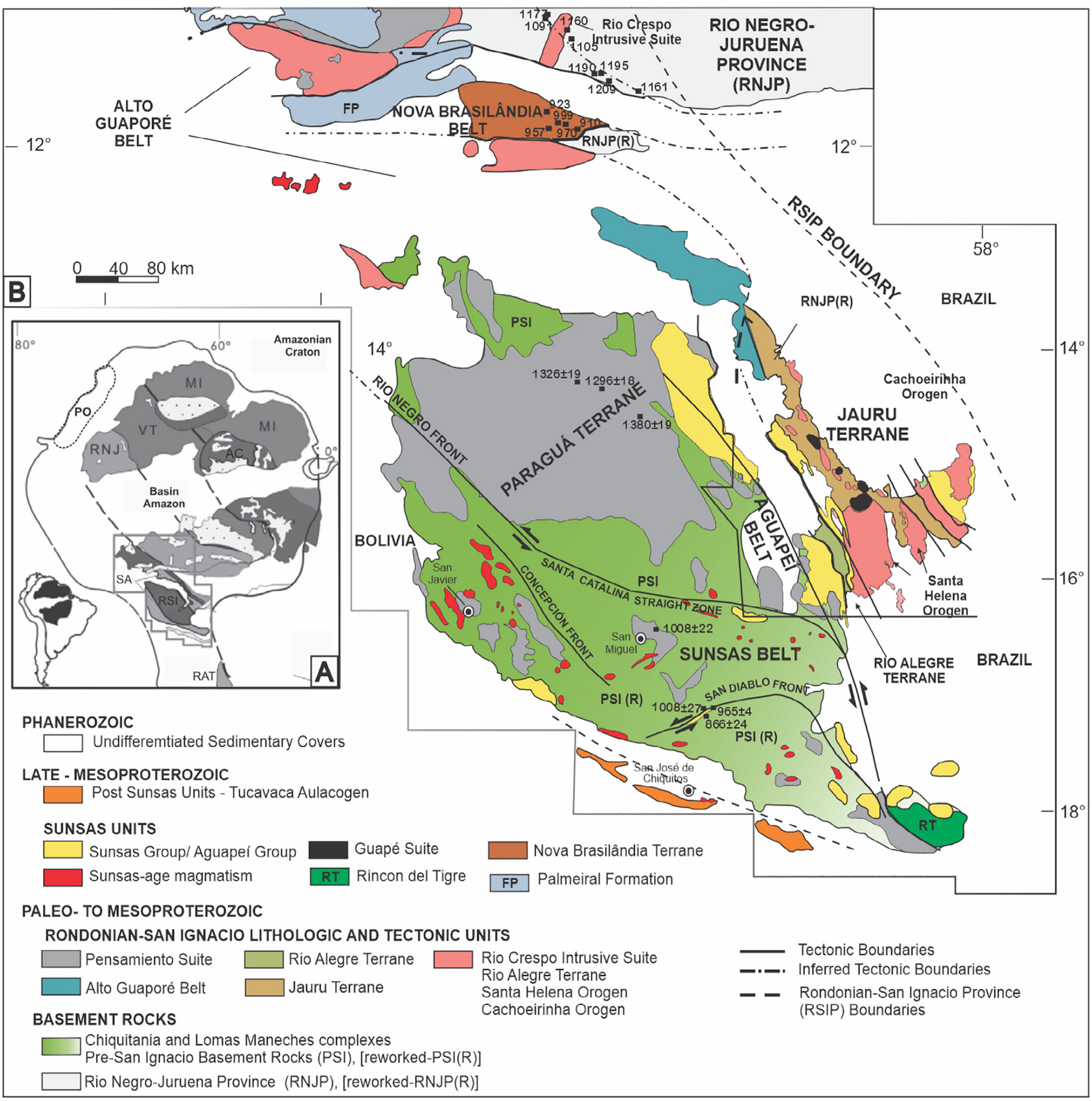

Fig. 1. (A) Schematic geotectonic compartmentation of the Amazonian Craton detaching the SW portion and the Sunsas Province (after Teixeira et al., 1989; Tassinari and Macambira, 1999, 2004; Tassinari et al., 2000) (modified from Cordani et al., 2000). AC - Amazônia Central (2.5 Ga), MI - Maroni-Itacaiúnas (2.2–1.95 Ga), VT - Venturi-Tapajós (1.95–1.8 Ga), RNJ - Rio Negro-Juruena (1.8–1.55 Ga), RAT – Rio Apa Terrane (2.0–1.5); RSI - Rondonian-San Ignacio (1.55–1.3 Ga); PO – Putumayo Orogen; and SA - Sunsas (1.3–1.0 Ga). (B) Schematic map of the SW Amazonian Craton with distribution of the main provinces, major orogens, terranes and belts, tectonic elements, and lithologic units in eastern Bolivia and western Brazil. Extracted and modified from Bettencourt et al. (2010).

Mesoproterozoic times (e.g., Tassinari and Macambira, 2004; Cordani and Teixeira, 2007). It consists of the 3.0–2.5 Ga older Amazonia Central Province surrounded by 2.2–2.0 Ga Paleoproterozoic juvenile and reworked terrains related to the Transamazonian orogenic collage (Fig. 1A) (e.g., Cordani et al., 2000; Tassinari and Macambira, 2004). The late Paleo- to early Mesoproterozoic transition recorded progressively younger magmatic accretions as evidenced by the 1.95–1.80 Ga Ventuari-Tapajós, 1.80–1.55 Ga Rio Negro-Juruena, 1.55–1.3 Ga Rondonian-San Ignacio and 1.3–1.0 Ga Sunsas provinces (e.g., Teixeira et al., 1989; Tassinari and Macambira, 1999, 2004). The latter includes rift stages, such as the Aguapeí aulacogen, and deposition of metasedimentary rocks related to the Mesoproterozoic Sunsas Group (e.g., Litherland et al., 1986; Saes and Leite, 1993; Geraldes et al., 2001; Table 1). A different proposal divides the craton into eight geochronological provinces (e.g., Santos et al., 2000, 2008): Carajás (3.0–2.5 Ga), Central Amazonian (~2.6 Ga), Transamazon (2.26–2.01 Ga), Tapajós-Parima (2.03–1.88 Ga), Rio Negro (1.82–1.52 Ga), Rondônia-Juruena (1.82–1.54 Ga), Sunsas (1.45–1.0 Ga) and K'Mudku (~1.2 Ga).

Following the first and main proposal model (e.g., Teixeira et al., 1989), a geochronological link between the Rio Apa Terrane (RAT) and the southernmost Amazonian Craton (Figs. 1A and 2) has been widely discussed (e.g., Lacerda-Filho et al., 2006; Cordani et al., 2010; Manzano et al., 2012; Brittes et al., 2013; Plens et al., 2013; Nedel et al., 2020; Teixeira et al., 2020). The RAT, located at the Brazil-Paraguay border, is a Paleoproterozoic crustal segment divided into western and eastern domains, formed of 1.95 Ga orthogneisses and 1.80 Ga granites, respectively (e.g., Lacerda-Filho et al., 2006, 2016, 2020; Cordani et al., 2010; Faleiros et al., 2016; Teixeira et al., 2020). Moreover, the pervasive regional deformation and medium-grade metamorphism at 1670 Ma and 1310 to 1270 Ma suggest a correlation between the Rio Apa Terrane and the Rio Negro-Juruena Province (Cordani et al., 2010; Faleiros et al., 2016; Teixeira et al., 2020). Therefore, the RAT may have been a fragmented and dispersed part of the Ventuari–Tapajós Province (Cordani et al., 2010; Faleiros et al., 2016; Teixeira et al., 2020).

2.1. Late Mesoproterozoic to tonian Sunsas Province

The Sunsas Province comprises the supracrustal and magmatic rocks generated and affected by the Sunsas orogeny (1.1–1.0 Ga), which is the last continental accretion recorded in the Amazonian Craton before its final tectonic stabilization (Figs. 1B and 2; e.g., Tassinari and Macambira, 2004; Cordani and Teixeira, 2007; Teixeira et al., 2010). This continental collision event was recorded in the Sunsas, Aguapeí, and Nova Brasilândia belts, developed along the Paraguá Terrane margins (1.74–1.32 Ga) (Fig. 1B; Table 1) (e.g., Bettencourt et al., 2010; Teixeira et al., 2010).

Litherland et al. (1986) and Litherland et al. (1989) undertook the initial lithostratigraphic studies of the Sunsas Province in eastern Bolivia. Soon after, Hoffman (1991) suggested a link between eastern Laurentia and SW Amazonia along the Grenville and Sunsas provinces during the early Neoproterozoic Rodinia assembly. Based on this, several geotectonic models were designed to take account the structural, igneous, and metamorphic features of igneous and supracrustal sequences that built the Amazonia and Laurentia borders (e.g., Santos et al., 2000; Tohver et al., 2004; Boger et al., 2005).

Considering the Rodinia scenario, the timing of magmatic events is important to highlight the Sunsas Province age-correlation with the Meso- to Neoproterozoic Putumayo orogenic belt (1.45–0.98 Ga) (Fig. 1A). The Putumayo Orogen is exposed as inliers in northwestern South America, within the northern Andes of Colombia, Peru and Venezuela (Fig. 1A) (e.g., Ibañez-Mejia et al., 2011; Ibañez-Mejia, 2020). The orogen evolved from a pericratonic fringing-arc system outboard of leading Amazonia margin developed from ~1.3 Ga to 1.1 Ga, followed by two metamorphic episodes at 1.05–1.01 Ga and ~0.99 Ga (Ibañez-Mejia, 2020). This age-correlation can provide key information about the Amazonia Meso- to early Neoproterozoic tectonics. Moreover, it contributes

Table 1
Geochronological and isotopic data from the Sunsas Province magmatism, SW Amazonian Craton (Teixeira et al., 2010; Quadros et al., 2020).

Tectonic Unit	Granite	References	U–Pb	Rb–Sr	Sm–Nd		Tectonic setting
			Ages (Ma)	Ages (Ma)	Tdm (Ga)	$\varepsilon_{Nd}(t)$	
SUNSAS BELT	Taperas	Boger et al. (2005)	1076 ± 18				Magmatic arc
		Vargas-Mattos (2010)	1047 ± 24		1.71	−5.82	
	Casa de Piedra	Litherland et al. (1986)		1005 ± 12			
		Darbyshire (2000)			1.92	−4	
		Vargas-Mattos (2010)	1089 ± 30			−4.94	
	El Carmem	Vargas-Mattos (2010)	1071 ± 34		1.80	−5.03	
	Naranjito		1048 ± 19		1.75		
	Primavera		1.08 Ga		1.66	−0.59	
	Señoritas	Isla-Moreno (2009)	1004 ± 1				
AGUAPEÍ BELT	Guapé	Teixeira et al. (1989)		835 - 900			Aulacogen setting
	Guapé	Menezes et al. (1993)		950 ± 40			
	São Domingos	Geraldes (2000)	936 ± 26		2.21	−7.1	
	São Domingos		930 ± 12			−7.6	
	Sararé	Araújo-Ruiz (2003)	907 ± 18				
	Sararé	Ruiz (2005)			2.9	−4.97	
NOVA BRASILÂNDIA BELT	Rio Branco suite	Quadros et al. (2020)	1113 ± 7				Magmatic emplacement arc – back-arc system formation
			1112 ± 2				
			1119 ± 3				
			1106 ± 3				
	São Domingos	Siqueira (2015)	928 ± 5		1.58	−2.9	Collision and crustal thickening (High-grade metamorphic and migmatization)
	Granito Rio Branco	Rizzotto (1999)	1113 ± 53				
	Granitos sin-tectônicos		1110 ± 8				
	Metagabro		1110 ± 10				
	Granito Rio Pardo		1005 ± 41				

with important implications for the geodynamic significance and the understanding of role played by the Amazonian Craton during the amalgamation of the Rodinia supercontinent (Ibañez-Mejia, 2020).

2.1.1. Sunsas belt

The Sunsas belt is an NW–SE trending 600 km long belt that comprises the rock assemblage exposed in the western portion of the Sunsas Province (Litherland et al., 1986, 1989). Its final structuring occurred during the Sunsas orogeny (Litherland et al., 1986, 1989; Tassinari and Macambira, 2004; Cordani and Teixeira, 2007; Teixeira et al., 2010). The stratigraphic configuration is formed of the 1.76–1.68 Ga Chiquitania and 1.81–1.65 Ga Lomas Maneches complexes, that form the Paraguá Terrane, <1.69 Ga San Ignacio Group, 1.37–1.28 Ga Pensamiento Suite, 1.2–1.1 Ga Sunsas Group, and 1.1–1.0 Ga magmatism (Figs. 2 and 3) (Litherland and Bloomfield, 1981; Litherland et al., 1986; Teixeira et al., 2010).

The Sunsas belt is compartmentalized by transpressive shear zones, namely the Rio Negro, Santa Catalina, Concepción, and San Diablo fronts (Fig. 3). The Rio Negro and Santa Catalina fronts record the tectonic transport from southwest to northeast of the Sunsas belt. The San Diablo front is a curvilinear dextral shear zone related to tectonic northward stress whereas the Rio Negro front resulted from the near frontal, tangential, SW–NE directed collage (Litherland et al., 1986; Nedel et al., 2017). The Concepción front separates a pervasively deformed domain in the SW from a non-pervasive deformation domain in the NE (Litherland et al., 1986). These continental-scale shear zones were developed at 1.08–1.04 Ga along the southern margin of the Paraguá Terrane affecting the oldest basement and the sedimentary covering of the Sunsas Group (<1200 Ma maximum depositional age) (Fig. 2; Litherland et al., 1986; Teixeira et al., 2010; Nedel et al., 2017). The shear zones crustal weakness acted as channels for the magma ascent controlling the Sunsas high-K granites emplacement within the Paleo- to Mesoproterozoic basement (Litherland and Bloomfield, 1981; Litherland et al., 1986; Teixeira et al., 2010). Furthermore, these structures also control occurrences of gold in Mato Grosso,

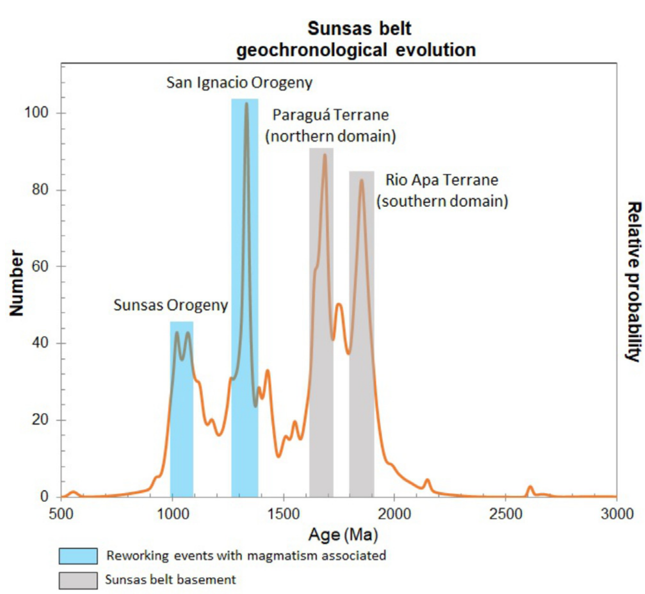

Fig. 2. Histogram of $^{207}Pb/^{206}Pb$ zircon ages from the Sunsas belt showing the geochronological evolution of Paleoproterozoic basement reworked during the San Ignacio and Sunsas orogenies. Data compiled from Boger et al. (2005), Santos et al. (2008), Vargas-Mattos (2010), Nedel et al. (2020), and Redes et al. (2020).

Brazil (e.g., Fernandes et al., 2006) and in the Don Mario mineral district in Bolivia (Teixeira et al., 2010).

3. Analytical methods and procedures

3.1. Geological sampling and petrography

A total of eleven granitic plutons from the Sunsas belt in Southeastern Bolivia were sampled and dated (Fig. 3; Table 2). The plutons were chosen based on geological mapping of eastern Bolivia performed by Servicio Geologico de Bolivia during the development of the Proyecto Precambrico, in the 1970s and 1980s (Litherland et al., 1986). Rock outcrops are scarce in the study region due to intense chemical weathering, thickness of soil layers and forest cover. Systematic thin sections perpendicular to foliation were obtained from the granite samples. Petrographic descriptions were done at the Microscopy Laboratory of the Institute of Geosciences of Universidade de Brasília (Brazil).

3.2. Zircon and monazite U–Pb isotopes

U–Pb isotopic analyses were performed on zircon from eleven granite samples (LA14, TAP02, SM10, ID02, ID06, ID08, ID09, ID11, ID18, SR20, SM07) and monazite grains from two samples (ID06, ID08) conducted on a Thermo Finnigan Neptune MC-ICP-MS, coupled with a New Wave UP213 Nd: YAG laser (λ = 213 nm) at the Laboratory of Geochronology of Universidade de Brasília, following the procedures described by Bühn et al. (2009). Measurements consisted of spot analyses.

In order to extract zircon and monazite grains, samples were first processed in a rock crusher, producing chips roughly 3–5 cm in size. Samples were then processed in a Selfrag high voltage laboratory equipment, with a voltage of 130 kV and a frequency of 3 Hz. Zircon and monazite grains were concentrated using a pan to separate the heavy mineral fraction and a Franz was then used to remove the magnetic fraction. Zircon and monazite grains were handpicked using a binocular microscope. Grains were mounted in epoxy mounts and polished to create a smooth surface. HNO_3 (ca. 2%) was used to clean the surface of the mounts. Backscattered electron images (BSE) of the zircon grains were taken with a FEI-Quanta 450 scanning electron microscope, working at 20–25 kV, at Universidade de Brasília, in order to characterize grain zoning.

U–Pb analyses on zircon grains were carried out by the standard-sample bracketing method (Albarède et al., 2004), using the GJ-1 standard zircon (Jackson et al., 2004) in order to quantify the amount of ICP-MS fractionation. The tuned masses were ^{238}U, ^{207}Pb, ^{206}Pb, ^{204}Pb, and ^{202}Hg. The integration time was 1 s, and the ablation time was 40 s. A 30 μm spot size was used, and the laser setting was 10 Hz and 2–3 J/cm^2. For monazite, a laser beam diameter of 25 μm at 10 Hz and ~2.4 J/cm^2 was implemented with one analytical spot per monazite crystal. Two to four unknown grains were analyzed between GJ-1 analyses. $^{207}Pb/^{206}Pb$ and $^{206}Pb/^{238}U$ ratios were time corrected. The raw data were processed off-line and reduced using an Excel worksheet (Bühn et al., 2009) with the aid of "Chronus" software (Oliveira, 2015). During the analytical sessions, zircon standard 91500 (Wiedenbeck et al., 2004) was also analyzed as an external standard. Zircon ages were calculated using ISOPLOT v.3 (Ludwig, 2003), with isotopic ratio errors presented at 2 SE. The internal laboratory monazite (Chaves et al., 2010) and 44069 monazites (424.86 ± 0.36 Ma; Aleinikoff et al., 2006) were used as the primary and external standard for monazite analyses, respectively.

Common ^{204}Pb was monitored using the ^{202}Hg and (^{204}Hg + ^{204}Pb) masses. Common Pb corrections were not done due to weak signals of ^{204}Pb (<30 cps) and high $^{206}Pb/^{204}Pb$ ratios.

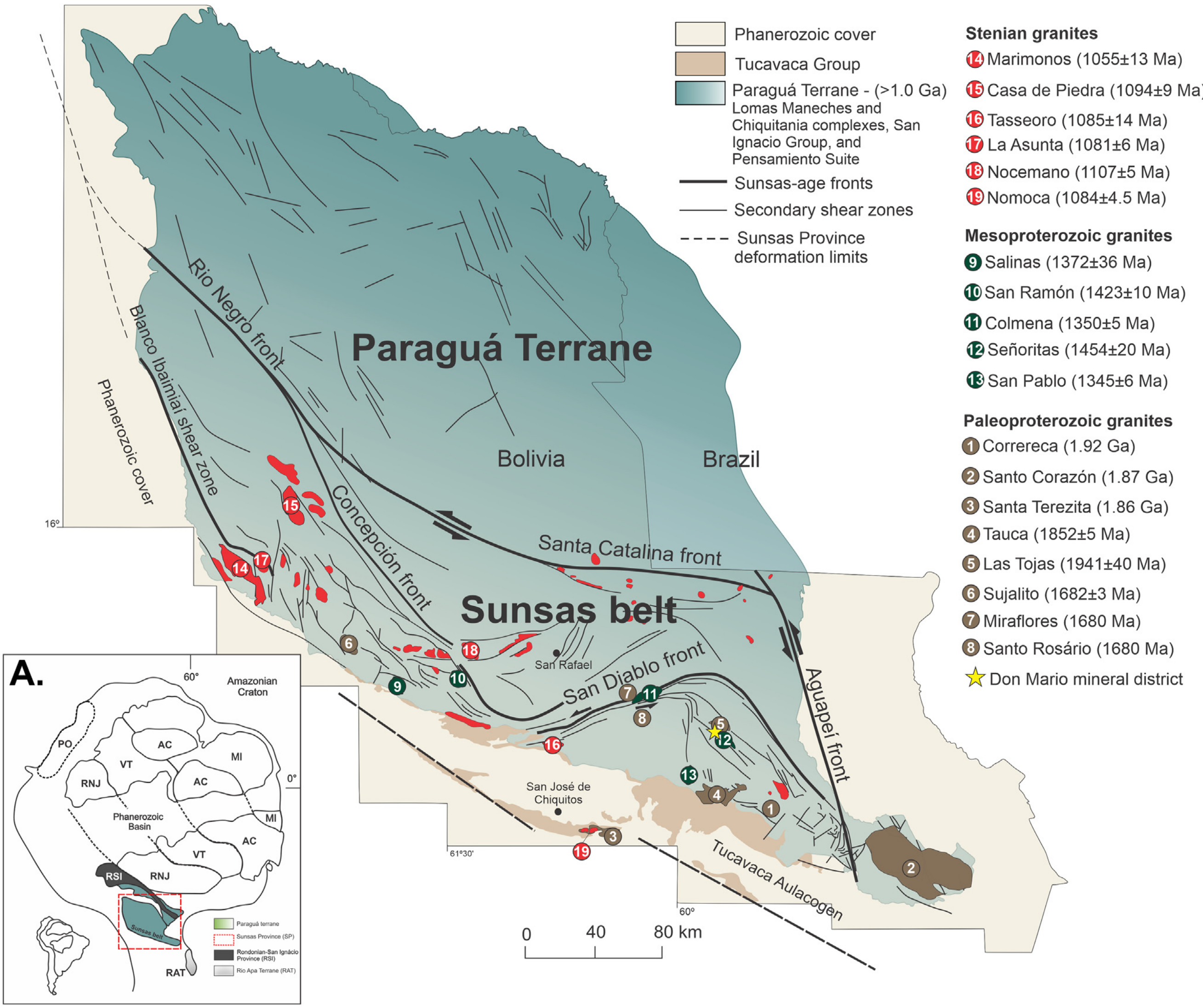

Fig. 3. (A) Schematic geotectonic compartmentation of the Amazonian Craton detaching the SW portion and the Sunsas Province (after Teixeira et al., 1989; Tassinari and Macambira, 1999, 2004; Tassinari et al., 2000) (modified from Cordani et al., 2000); (B) Schematic geological map for the Paraguá Terrane, SW Amazonian Craton, with focus on the Sunsas belt and the studied pluton's location.

Table 2
Studied granites from the Sunsas belt in southeastern Bolivia.

Pluton	Sample	Classification	Area 1:250000*	Coordinates - UTM	
				Latitude	Longitude
Marimonos	MR11	Granite	Concepcion CUAD, SE 20-3/SE 20-2	514,849	8,197,726
San Ramón	ID11	Granite		536,428	8,176,968
Sujalito	SR20	Granite		568,896	8,161,116
Tasseoro	TAS 15	Granite	San José de Chiquitos CUAD, SE 20-8/SE20-7	734,892	8,075,813
Colmena	IM34	Granite		772,148	8,101,574
Salinas	SM10	Monzogranite		622,464	8,120,572
San Pablo	ID02	Monzogranite	Santo Corazón CUAD, SE 21-5/SE 21-9	193,169	8,058,223
Señoritas	ID06	Two-mica granite		213,825	8,081,030
Las Tojas	ID08	Two-mica granite		210,690	8,090,872
Tauca	ID09	Granodiorite		217,672	8,038,242
Casa de Piedra	ID18	Monzogranite	Monte Verde CUAD SD 20-15	554,208	8,243,651

* Bolivian cartographic base developed by the Precambrian Project at 1970's.

Reported errors are propagated by quadratic addition $[(2SD^2 + 2SE^2)^{1/2}]$ (SD = standard deviation; SE = standard error) of external reproducibility and within-run precision. External reproducibility is represented by the standard deviation obtained from repeated analyses (~1.1% for $^{207}Pb/^{206}Pb$ and up to ~2% for $^{206}Pb/^{238}U$) of the GJ-1 zircon standard during the analytical

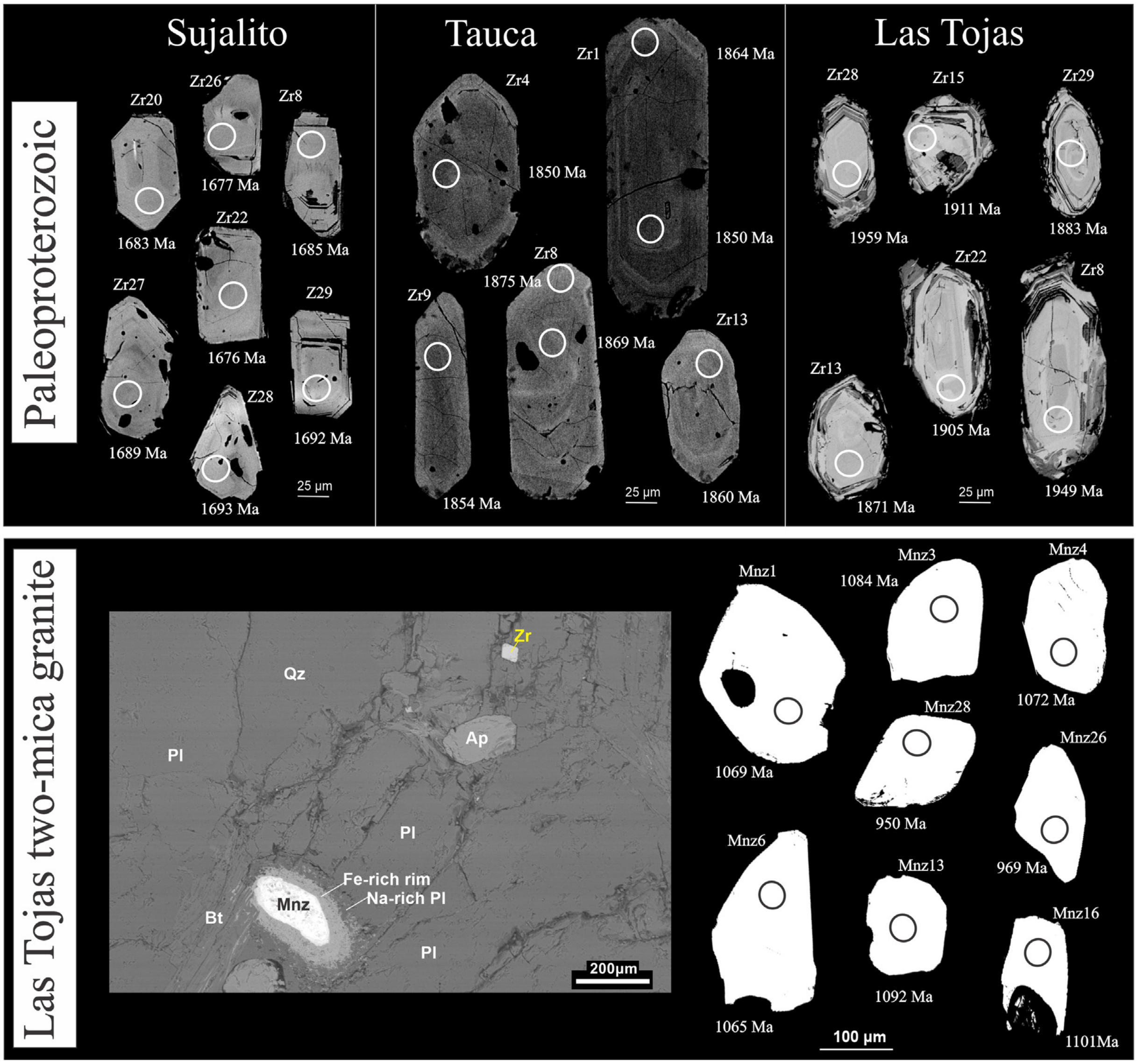

Fig. 4. Representative cathodoluminescence (CL) and backscattered electron (BSE) images for zircon and monazite grains from the Sunsas belt Paleoproterozoic granitic plutons. The Sujalito sample displays two morphological populations; one as rounded zircon crystals, lengths of 100–300 µm, aspect ratio of 2:1; the other as prismatic elongated crystals, lengths of 200–300 µm, aspect ratio of 3:1. Both populations show internal structures with faint concentric oscillatory zoning or unzoned crystals. Many inclusions and fractures are also observed. The Tauca sample shows two morphological populations: one as rounded zircon, lengths of 100–300 µm, aspect ratio of 2:1; the other as prismatic elongated crystals, lengths of 200–300 µm, aspect ratio of 3:1. Both populations display faint concentric oscillatory zoning or unzoned crystals. Many inclusions and fractures are also observed. The Las Tojas sample contains fractured subhedral rounded and prismatic zircon. Prismatic grains have lengths of 100–200 µm, aspect ratio of 1:1 and rounded crystals 90–190 µm, aspect ratio of 2:1. In BSE images, all crystals have xenoscrystic internal structures, cores present faint oscillatory zoning truncated by growth of zoned rims, up to 20 µm. In general, cores are lighter than rims and have not well marked limits. There is evidence of resorption and recrystallization.

sessions and the within-run precision is the standard error calculated for each analysis. Concordia diagrams (2 SE ellipses), probability density plots and weighted average ages were calculated using the Isoplot-3/Ex software (Ludwig, 2008).

4. Results of U–Pb dating

4.1. Paleoproterozoic granites

The older magmatism is represented by granodiorite and granite emplaced in the southern part of the Sunsas belt (Fig. 3). The Las Tojas two-mica granite (30%–39% plagioclase, 25%–31% K-feldspar, 20%–30% quartz and 8%–15% mica) presents incipient foliation that reflects the host NW–SE tectonic transcurrent shear zone. The Tauca granodiorite (38%–42% plagioclase; 29%–32% quartz; 15%–18% K-feldspar; and 10%–15% biotite) and Sujalito granite (33%–35% quartz; 29%–35% K-feldspar; 25%–33% plagioclase; and 3%–5% biotite) exposures are very weathered, hampering recognition of deformation structures. However, the primary mineral assemblage remains partially preserved.

All zircon grains from the Las Tojas, Tauca, and Sujalito samples are prismatic crystals with lengths of 100–300 µm, aspect ratios of 2:1 and 3:1 (Fig. 4). The backscattered electron (BSE) images show magmatic zoning with recrystallization fronts and zones (Fig. 4) (e.g., Corfu et al., 2003).

The Sujalito granite yielded an upper intercept age of 1685 ± 6 Ma (Fig. 5A). Seven concordant zircon grains with moderate Th/U ratios between 0.28 and 0.45 yielded a Concordia age of 1682 ± 3 Ma (Fig. 5B), interpreted as the crystallization age. The Las Tojas two-mica granite shows an upper intercept age of 1941 ± 40 Ma (Fig. 5E) obtained from zircon cores with moderate

Th/U ratios of 0.23 to 0.59. Zircon rims with Th/U values of 0.16 and 0.26 have younger $^{207}Pb/^{206}Pb$ ages of 1271 Ma and 1215 Ma (Table 2). Thirty monazite crystals from the Las Tojas two-mica granite were also dated. Monazite crystals display morphological features of igneous growth and occur as inclusions in feldspar and white mica (Fig. 4). They yielded an upper intercept age of 992 ± 41 Ma with reversely discordant standards (Fig. 6A). This occurs due to excess of ^{206}Pb resulting from preferential uptake of ^{230}Th during crystal growth, making the $^{206}Pb/^{238}Pb$ ratios plot above concordia in the diagram (Schärer, 1984; Parrish, 1990). In this case, the $^{207}Pb/^{235}U$ ages can provide more precise information about monazite generation (Parrish, 1990). Therefore, the weighted mean of $^{207}Pb/^{235}U$ ages of 1079 ± 14 Ma with the 95% confidence is considered as the best estimate for the monazite crystallization age (Fig. 6B). In turn, the Tauca granodiorite displays a discordant upper intercept age of 1856 ± 4.4 Ma (Fig. 5C) with Concordia age of 1852 ± 5.3 Ma (Fig. 5D), interpreted as the zircon crystallization age.

4.2. Mesoproterozoic granites

The Colmena granite is hosted along the San Diablo front within the Chiquitania Gneissic Complex. It is strongly deformed, displaying E–W lineation compatible with the Sunsas Group deformation and secondary shear zones developed during the Sunsas tectonic activity in the region (Litherland et al., 1989). The Colmena pluton

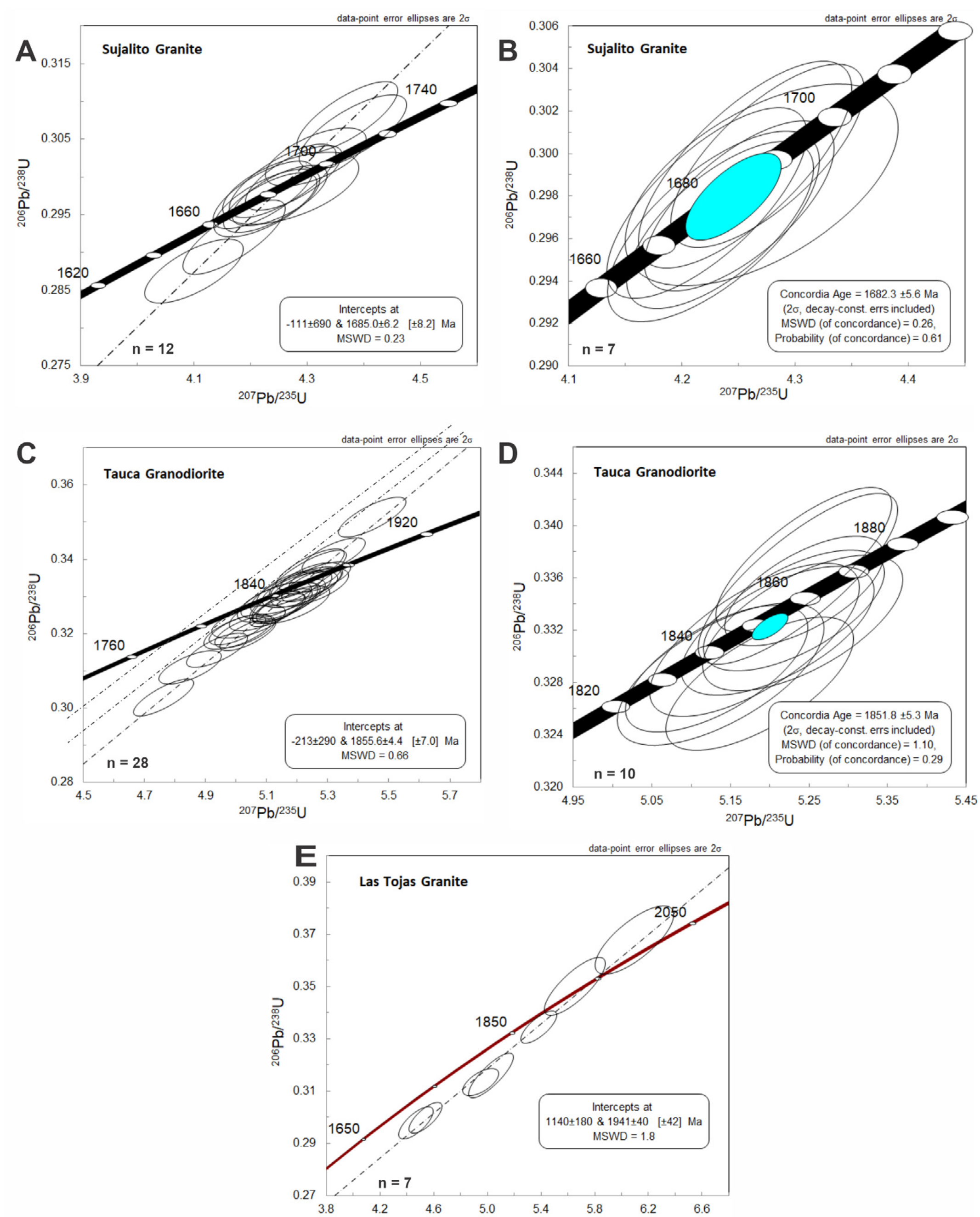

Fig. 5. (A) Concordia diagram and (B) concordant age for U–Pb zircon data from the Sujalito pluton; (C) Concordia diagram and (D) Concordant age for U–Pb zircon data from the Tauca pluton; (E) Concordia diagram for U–Pb zircon from the Las Tojas granitic pluton. From Table 3 and Supplementary Data, Table S1.

is formed of K-feldspar (30%–35%) + plagioclase (20%–25%) + qua rtz (20%–25%) + biotite (10%–15%). The San Ramón granite exhibits incipient foliation marked by the biotite orientation. The Señoritas two-mica granite occurs as parallel lenses hosted in the WNW–ESE-trending mica-schist sequence related to a gold mineralized shear zone in the Don Mario mineral district (e.g., Litherland et al., 1986). White mica and K-feldspar grains present monazite inclusions, which indicate cogenetic generation. The Salinas and San Pablo monzogranites mineral assemblage is characterized by the presence of hornblende and pyroxene and it mainly consists of plagioclase (40%–44%) + K-feldspar (24%–29%) + quartz (20%–27%) + biotite (3%). The mafic minerals display adcumulate texture, sometimes producing a banded mineral structure.

The zircon grains from these samples are prismatic, measuring 50 to 300 μm, with aspect ratios of 2:1 and 3:1. The BSE images show unzoned to oscillatory and banded zircon internal texture (Fig. 7). Grains with recrystallization zones and no internal texture mainly occur in the San Pablo and Colmena granites crystals (Fig. 7). The zircon crystals usually have well-delimited zoning between core and rim and show disruption of concentric oscillatory zoning, typical of metamorphic recrystallization fronts and zones (see San Ramón, Fig. 7) (e.g., Corfu et al., 2003).

The zircon cores from the San Pablo monzogranite have moderate Th/U values, from 0.42 to 0.71, and yielded an upper intercept age of 1345 ± 6 Ma (Fig. 8A), interpreted as the crystallization age. Inherited zircon core of 1848 Ma and overgrowth rim age of 1345 Ma is also recorded (Fig. 7 and Supplementary Data, Table S1; Corfu et al., 2003). Prismatic zircon grains from the Salinas monzogranite display an upper intercept age of 1372 ± 36 Ma (MSWD = 11), interpreted as the minimum crystallization age, taking account of the crystals Pb-loss (Fig. 8B). Six inherited zircon grains with typical disruption of internal structures (Figs. 7 and 8B; Corfu et al., 2003) yielded an older upper intercept age of 1684 ± 110 Ma (Figs. 7 and 8B). The San Ramón granite shows a discordant upper intercept age of 1423 ± 10 Ma (Fig. 8C) on unzoned grains and zircon rims with moderate Th/U ratios between 0.22 and 0.48. Inherited zircon cores present $^{207}Pb/^{206}Pb$ ages between 1815 Ma and 1876 Ma, with Th/U ratios varying from 0.07 to 0.36. For instance, zircon 38 (see Fig. 7) from San Ramón has an inherited core dated at 1826 Ma, with low Th/U ratio of 0.07, while its overgrowth rim is dated at 1405 Ma, with Th/U ratio of 0.28.

The Colmena granite shows an upper intercept age of 1350 ± 5 Ma (Fig. 8D) obtained from zircon cores with moderate Th/U ratios between 0.15 and 0.68, interpreted as the crystallization age. Inherited zircon grains with ages of 1635 Ma and 1761 Ma were also found in the Colmena granite. Due to high discordance, 34% and 9%, respectively, both ages may represent only one age population. The Señoritas two-mica granite displays two $^{207}Pb/^{206}Pb$ ages in the zircon cores (Figs. 7 and 8E). Zircon grains with aspect ratio of 2:1 yielded an older discordant upper intercept age of 1954 ± 51 Ma. Zircon grains with aspect ratio of 3:1 yielded a younger upper intercept age of 1454 ± 20 Ma, with a concordant age of 1415 ± 30 Ma, interpreted as the best estimate for the crystallization age. Th/U ratios overlap in both age groups. Monazite from the Señoritas granite was also dated (Table 3). The BSE images show small and faceted monazite, typical of igneous crystals (Fig. 7) (Williams et al., 2007). Specifically, U–Pb monazite results

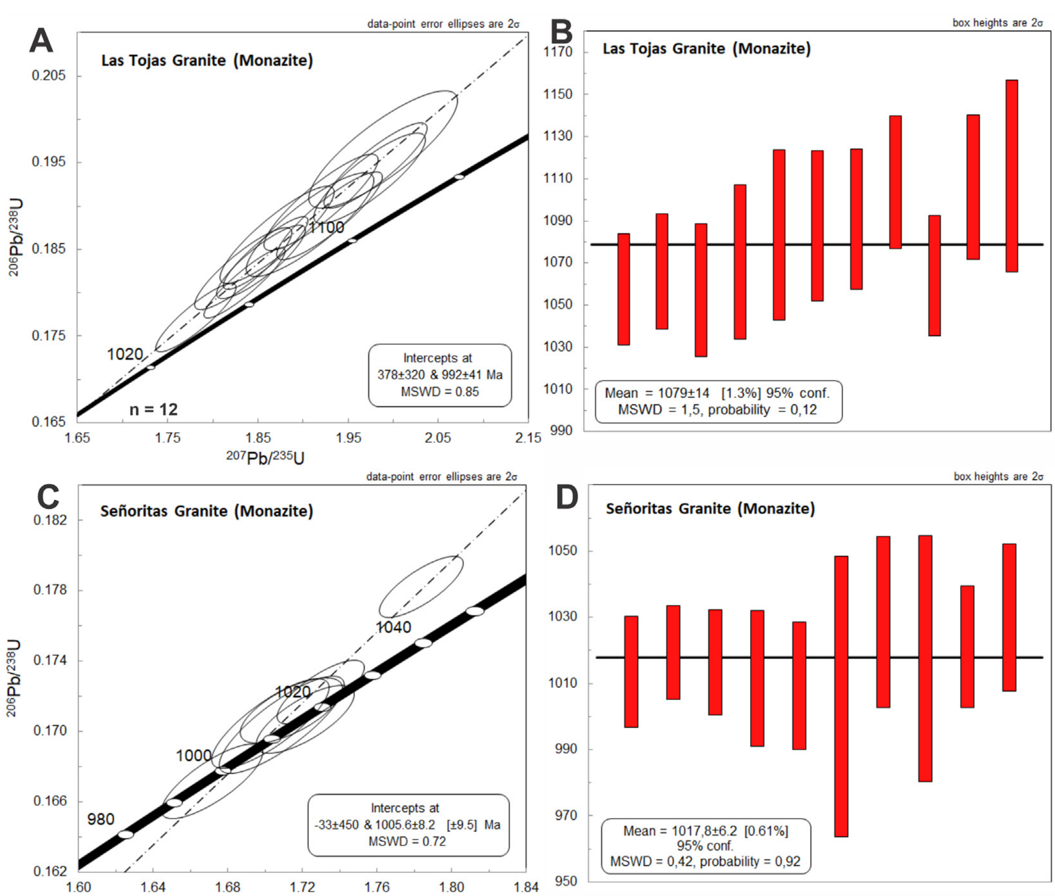

Fig. 6. U–Pb monazite data. (A) Concordia diagram and (B) weighted mean of $^{207}Pb/^{235}U$ ages from the Las Tojas granite, (C) Concordia diagram and (D) weighted mean of $^{207}Pb/^{235}U$ ages from the Señoritas granite.

show an upper intercept age of 1006 ± 8 Ma (Fig. 6C). The weighted mean of $^{207}Pb/^{235}U$ ages with 95% confidence yielded a slightly older age of 1018 ± 6 Ma, considered the best estimate age for monazite crystallization (Fig. 6D). Thus, the Señoritas granite records a complex evolution, with zircon generated at 1.95 Ga and 1.45 Ga, and a monazite generation at 1018 ± 6 Ma.

4.3. Stenian granites

The Tasseoro, Casa de Piedra and Marimonos granodioritic to monzogranitic intrusions are emplaced in the western and southern portions of the Sunsas belt and represent the youngest studied igneous rocks. These granitic plutons mainly occur as lens-shaped intrusions controlled by NW–SE and E–W structures, often with deformed borders and incipient foliation marked by biotite orientation (Fig. 3). The mineral assemblage is formed of plagioclase (20%–30%) + K-feldspar (25%–35%) + quartz (30%–40%) + biotite (5%–15%). Amphibolite and pyroxenite xenoliths are found in the Casa de Piedra intrusion.

The zircon grains from the Tasseoro, Casa de Piedra, and Marimonos granites are prismatic, 100 and 400 μm long with aspect ratios of 3:1 and 4:1. The zircon crystals from Casa de Piedra and Marimonos show cores with internal zoning surrounded by a thick homogeneous rim (Fig. 9). Zircon grains from Tasseoro have prismatic morphology but their unzoned internal texture likely indicates later recrystallization (Fig. 9) (e.g., Corfu et al., 2003).

The Tasseoro granite yielded an upper intercept age of 1085 ± 14 Ma (Fig. 10A), interpreted as the crystallization age. Four zircon crystals yielded a slightly older upper intercept age of 1168 ± 34 Ma (Fig. 10A), that can suggest analytical artefacts due to high Pb-loss. However, if we consider the last as a reliably age, the U–Pb data can indicate a crystallization age dispersion of

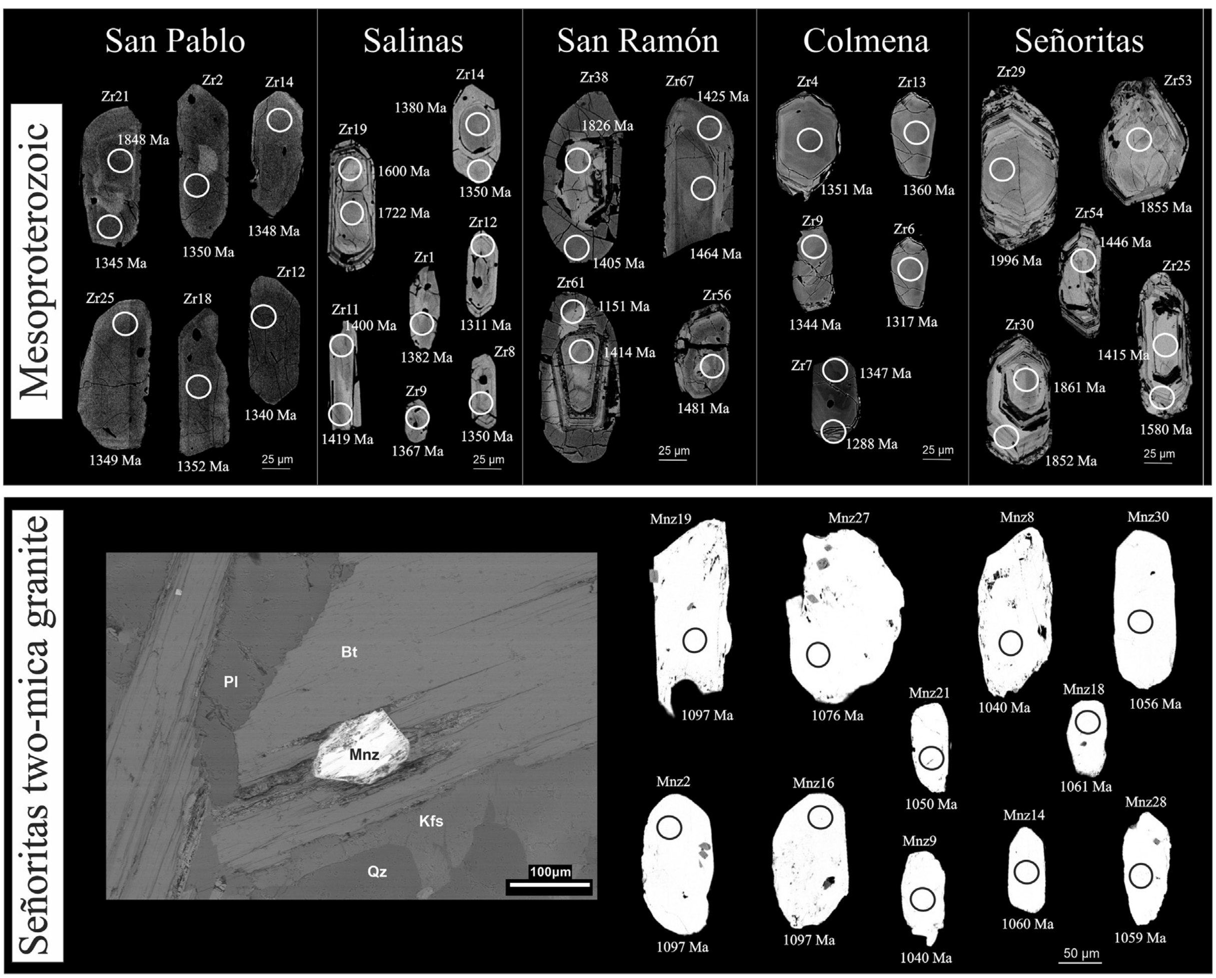

Fig. 7. Representative cathodoluminescence (CL) and backscattered electron (BSE) images for the zircon and monazite grains from Mesoproterozoic granitic plutons in the Sunsas belt. The San Pablo pluton sample shows rounded and elongated crystals with subhedral shapes measuring between 80 and 320 μm. BSE images show unzoned internal structures. Some crystals have light-colored cores without age variation. The Salinas intrusion sample presents prismatic and elongated zircon grains, measuring 50 to 200 μm, aspect ratio of 3:1. The crystals display some inclusions and fractures. BSE images show unzoned to faint oscillatory zoning internal structures with thin portions of oscillatory zoning. The San Ramón sample contains rounded grains with subhedral shapes, measuring between 80 and 300 μm, aspect ratio of 2:1. Most crystals are very fractured and present inclusions. BSE images show complex internal structures with oscillatory and banded zoning, in which some layers are up to 10 μm thick, and BSE-dark zircon cores, indicating high Pb concentration. These crystals usually have well-delimited zoning between core and rim and show disruption of concentric oscillatory zoning, typical of late and post-magmatic cooling. Some crystals with unzoned internal structure are also observed. The Colmena intrusion sample displays two zircon populations, different in terms of external appearance and internal geometry: such as: prismatic zircon grains of 40 to 120 μm that preserve igneous internal zoning structures, and rounded zircon grains of 90 to 190 μm, aspect ratios of 2:1 and 1:1. BSE images show uniform unzoned to faint zoning internal structures and evidence for resorption and recrystallization of the grains. Thin portions of rim overgrowth with oscillatory zoning indicate conditions of medium to high temperature metamorphism. The Señoritas pluton sample contains three morphological populations with different internal geometry: (1) Rounded subhedral crystals, lengths of 100–150 μm, aspect ratio of 1:1, with complex internal structures of xenocrystic cores with chaotic zoning and growth of zoned rims. Core and rim limits are not well defined. (2) Prismatic subhedral crystals measuring 100 to 200 μm, aspect ratio of 2:1, with faint oscillatory zoning commonly truncated by growth of thin zoned rims. (3) Less common, prismatic grains, 100–120 μm, aspect ratio of 2:1. Regular oscillatory zoning and evidence for resorption.

~60–80 Ma, as discussed later. The Casa de Piedra monzogranite shows three upper intercept ages: 1763 ± 35 Ma (Fig. 10B) yielded by zircon cores with Th/U ratios between 0.14 and 1.12; prismatic zircon grains (2:1) with relatively low to moderate Th/U ratios (0.09 and 0.45), yielded an upper intercept age of 1278 ± 96 Ma (Fig. 10B), with one concordant zircon crystal of 1279 ± 70 Ma. A specifically group of prismatic zircon grains yielded an upper intercept age of 1094 ± 9 Ma (Fig. 10C), interpreted as the crystallization age. Lastly, fifteen homogeneous zircon cores and overgrowth rims from the Marimonos granite yielded an upper intercept age of 1060 ± 9 Ma, also interpreted as the crystallization age (Fig. 10E). Moreover, four inherited zircon cores with internal zoning yielded an upper intercept age of 1388 ± 28 Ma (Fig. 10D), with one concordant zircon core of 1382 ± 24 Ma. Also, three older inherited zircon cores with magmatic zoning display an upper intercept age of 1633 ± 41 Ma (Fig. 10D), with a concordant age of 1623 ± 15 Ma. Thus, the 1055 ± 13 Ma Marimonos granite records at least two inheritance ages from magmatic episodes around 1.62 Ga and 1.38 Ga.

5. Discussion

5.1. Paleoproterozoic source correlations

The Paleoproterozoic Las Tojas granite (1941 ± 40 Ma; Fig. 5E) and Tauca granodiorite (1855 ± 4 Ma; Fig. 5D) are exposed in the southern portion of the San Diablo front. This Orosirian calc-alkaline magmatism documented in the south and extreme south

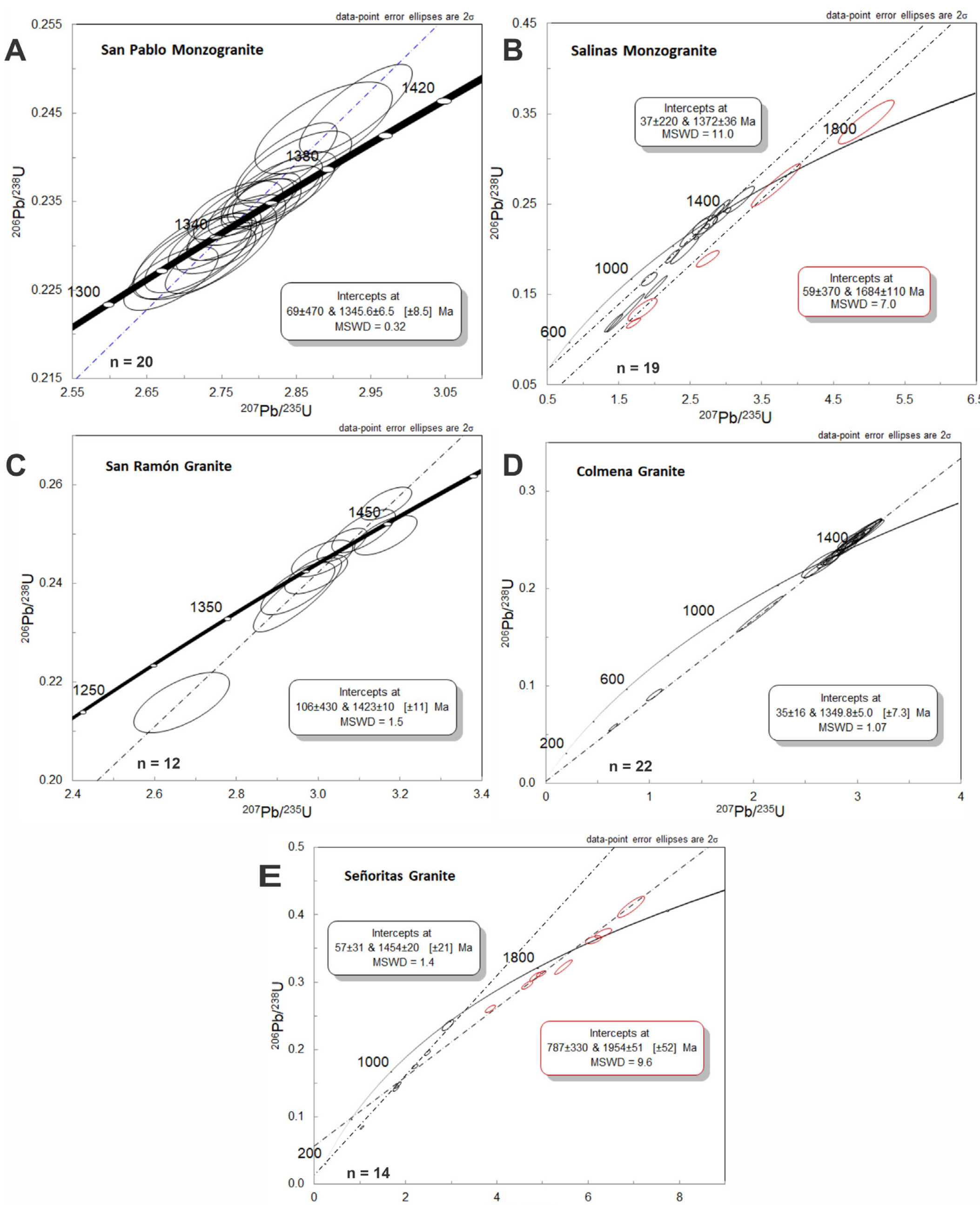

Fig. 8. Concordia diagram for U–Pb zircon data from the (A) San Pablo, (B) Salinas, (C) San Ramón, (D) Colmena, and (E) Señoritas granitic plutons. From Table 3 and Supplementary Data, Table S1.

Table 3
U–Pb monazite data from the granitic plutons of the Sunsas belt in southeastern Bolivia.

Las Tojas granite Sample	Spot	^{204}Pb cps	^{206}Pb mV[1]	Th/U	^{206}Pb/^{204}Pb	1 s%	^{207}Pb/^{206}Pb	1 s %	^{207}Pb/^{235}U	1 s %	^{206}Pb/^{238}U	1 s %	Rho	^{207}Pb/^{206}Pb	2 s abs	^{206}Pb/^{238}U	2 s abs	^{207}Pb/^{235}U	2 s abs	% U–Pb disc[2]
ID08	003-MZ1	173	0.0378	25.242	16,411	9.27	0.07501	0.47	1.781	1.02	0.1772	0.91	0.89	1069	19	1052	18	1038	13	1.59
ID08	005-MZ3	128	0.0227	28.684	61,734	80.06	0.07557	0.41	1.835	1.00	0.1812	0.91	0.91	1084	17	1074	18	1058	13	0.92
ID08	006-MZ4	156	0.0414	20.706	17,893	6.03	0.07514	0.46	1.859	1.04	0.1846	0.93	0.90	1072	18	1092	19	1066	14	−1.86
ID08	008-MZ6	133	0.0269	28.996	15,933	17.44	0.07488	0.57	1.834	1.20	0.1828	1.06	0.88	1065	23	1082	21	1058	16	−1.61
ID08	009-MZ7	134	0.0300	21.310	57,388	67.84	0.07478	0.66	1.871	1.39	0.1868	1.22	0.88	1063	26	1104	25	1071	18	−3.90
ID08	012-MZ10	509	0.0370	24.781	4780	6.41	0.07577	0.79	1.908	1.52	0.1880	1.30	0.86	1089	31	1110	27	1084	20	−1.96
ID08	015-MZ11	188	0.0369	25.906	13,175	5.50	0.07522	0.62	1.920	1.34	0.1905	1.19	0.89	1074	25	1124	25	1088	18	−4.64
ID08	016-MZ12	154	0.0257	32.397	12,041	9.51	0.07621	0.57	1.929	1.24	0.1890	1.10	0.89	1101	23	1116	23	1091	17	−1.37
ID08	017-MZ13	123	0.0208	29.263	12,737	10.35	0.07588	0.56	1.980	1.18	0.1948	1.03	0.88	1092	22	1147	22	1109	16	−5.06
ID08	018-MZ14	161	0.0299	27.016	12,333	6.17	0.07534	0.54	1.853	1.09	0.1836	0.94	0.87	1078	22	1087	19	1065	14	−0.85
ID08	020-MZ16	151	0.0313	23.718	13,368	4.46	0.07621	0.66	1.974	1.28	0.1933	1.09	0.86	1101	26	1139	23	1107	17	−3.51
ID08	028-MZ22	144	0.0330	25.126	15,828	6.59	0.07549	0.94	1.989	1.69	0.1966	1.41	0.83	1082	37	1157	30	1112	23	−6.99
Señoritas granite Sample	**Spot**	**^{204}Pb cps**	**^{206}Pb mV[1]**	**Th/U**	**^{206}Pb/^{204}Pb**	**1s%**	**^{207}Pb/^{206}Pb**	**1s %**	**^{207}Pb/^{235}U**	**1s %**	**^{206}Pb/^{238}U**	**1s %**	**Rho**	**^{207}Pb/^{206}Pb**	**2s abs**	**^{206}Pb/^{238}U**	**2s abs**	**^{207}Pb/^{235}U**	**2s abs**	**% U–Pb disc[2]**
ID06	018-MZ14	474	0.0959	12.488	12,970	3.38	0.07469	0.32	1.784	0.52	0.1783	0.40	0.78	1060	13	1058	8	1040	7	0.25
ID06	022-MZ18	422	0.1357	8.482	20,178	2.77	0.07471	0.48	1.714	0.65	0.1712	0.44	0.68	1061	19	1019	8	1014	8	3.95
ID06	032-MZ26	257	0.0543	20.353	14,542	5.34	0.07496	0.35	1.730	0.55	0.1723	0.43	0.77	1067	14	1025	8	1020	7	4.00
ID06	033-MZ27	315	0.0697	13.191	14,621	4.92	0.07526	0.42	1.722	0.62	0.1707	0.46	0.74	1076	17	1016	9	1017	8	5.52
ID06	034-MZ28	242	0.0740	9.469	19,902	4.62	0.07463	0.41	1.672	0.66	0.1672	0.52	0.78	1059	17	997	10	998	8	5.85
ID06	035-MZ29	352	0.0665	16.806	12,284	3.40	0.07484	0.46	1.709	0.80	0.1704	0.66	0.82	1064	18	1015	12	1012	10	4.68
ID06	036-MZ30	229	0.0531	18.095	15,723	4.69	0.07455	0.45	1.703	0.76	0.1705	0.61	0.80	1056	18	1015	11	1010	10	3.93

[1] Convertion factor from mV to CPS is 2,500,000.
[2] Discordance calculated as [1−(^{206}Pb/^{238}U age)/(^{207}Pb/^{206}Pb age)] × 100

of the Sunsas belt added to the geological configuration of the Amazonian Craton (Fig. 1B), suggests a 1.9–1.8 Ga petrogenetic link with the western domain of the Rio Apa Terrane (Figs. 2 and 3; Cordani et al., 2010; Faleiros et al., 2016; Redes et al., 2016, 2018; Plens, 2018; Nedel et al., 2020; Teixeira et al., 2020). It should be noted that the 1925 ± 32 Ma Correreca (Vargas-Mattos, 2010), 1874 Ma Santo Corazón (Redes et al., 2020) and 1861 ± 8 Ma Santa Terezita (Redes et al., 2018) granites are also exposed south of the San Diablo Front (Fig. 3). Furthermore, the widespread 1.9–1.8 Ga magmatism recorded in the Sunsas belt southern domain added to its transcurrent character with sinistral kinematic indicates the transport of older felsic crust from south to north during the Sunsas orogeny. Therefore, this older crust can be correlated to the Rio Apa Terrane which could be interpreted as a dispersed fragment subsequently reincorporated into the SW Amazonian Craton along the Sunsas belt as an allochthonous terrane (e.g., Cordani et al., 2010; Faleiros et al., 2016; Teixeira et al., 2020). In this scenario, the ~1.2 Ga zircon rims from 1.94 Ga Las Tojas two-mica granite would mark the last accretion of Rio Apa Terrane to the craton. The Neoproterozoic geodynamic interplay lasted until 1.1 Ga ago, recorded by some shared-components of a LIP event (e.g., Teixeira et al., 2015, 2020).

Moreover, time-correlation similarities indicate the Ventuari-Tapajós Province and the Rio Negro-Juruena Province as the best possibilities for a protracted link between the Amazonian Craton and the Rio Apa Terrane (e.g., Cordani et al., 2010; Faleiros et al., 2016; Teixeira et al., 2020). Another potential geochronological correlation could be the Paraguá Terrane protoliths and Rio Apa Terrane, given the age similarities (e.g., Cordani et al., 2010; Lacerda-Filho et al., 2016). However, Faleiros et al. (2016) do not ratify this last correlation due to distinct Nd isotope signatures (Lacerda-Filho et al., 2006; Santos et al., 2008; Matos et al., 2009; Cordani et al., 2010).

The 1682 ± 3 Ma Sujalito granite represents the older Paleoproterozoic basement exposed to the northwest of the San Diablo front. This Statherian magmatic episode can be correlated with the Chiquitania Complex that forms the Paraguá Terrane basement (Litherland et al., 1986; Teixeira et al., 2010). Therefore, the geochronological results suggest crustal reworking from distinct Paleoproterozoic sources in the Sunsas belt, one of ~1.9–1.8 Ga to the south of the San Diablo front and another of ~1.68 Ga to the north.

5.2. Mesoproterozoic correlations

The Calymmian to Ectasian (1.4–1.3 Ga) transition records the main magmatic rocks generation in the central portion of the Sunsas belt (Fig. 3). Five granitic intrusions were emplaced between 1.45 Ga and 1.35 Ga (Fig. 8). Specifically, the 1.37–1.34 Ga granites can be related to the Mesoproterozoic Pensamiento Suite that represents the final stage of the Rondonian-San Ignacio orogeny in the Paraguá Terrane (Fig. 2; Matos et al., 2009). This tectonic event resulted from the amalgamation of intra-oceanic magmatic arcs and accretionary prisms during a continental collision along the SW boundary of the Rio Negro-Juruena Province between 1.34 Ga and 1.32 Ga (e.g., Cordani and Teixeira, 2007; Bettencourt et al., 2010). Furthermore, the San Diablo front, developed ~1.0 Ga, may reflect inherited structures and weakness zones of the older collision between the Rio Apa (1.9–1.8 Ga western domain) and Paraguá terranes (1.6 Ga northern domain) during the San Ignacio orogeny, marked by the 1.35 Ga Colmena and San Pablo granites emplacement. Likewise, the 1.9–1.8 Ga and 1.68 Ga inherited zircon cores present in the 1.4–1.3 Ga old granitic intrusions also indicate crustal reworking of the Paleoproterozoic basement during the San Ignacio orogeny. The older 1.45–1.42 Ga San Ramón and Señoritas granites may be related to the Santa Helena Orogen,

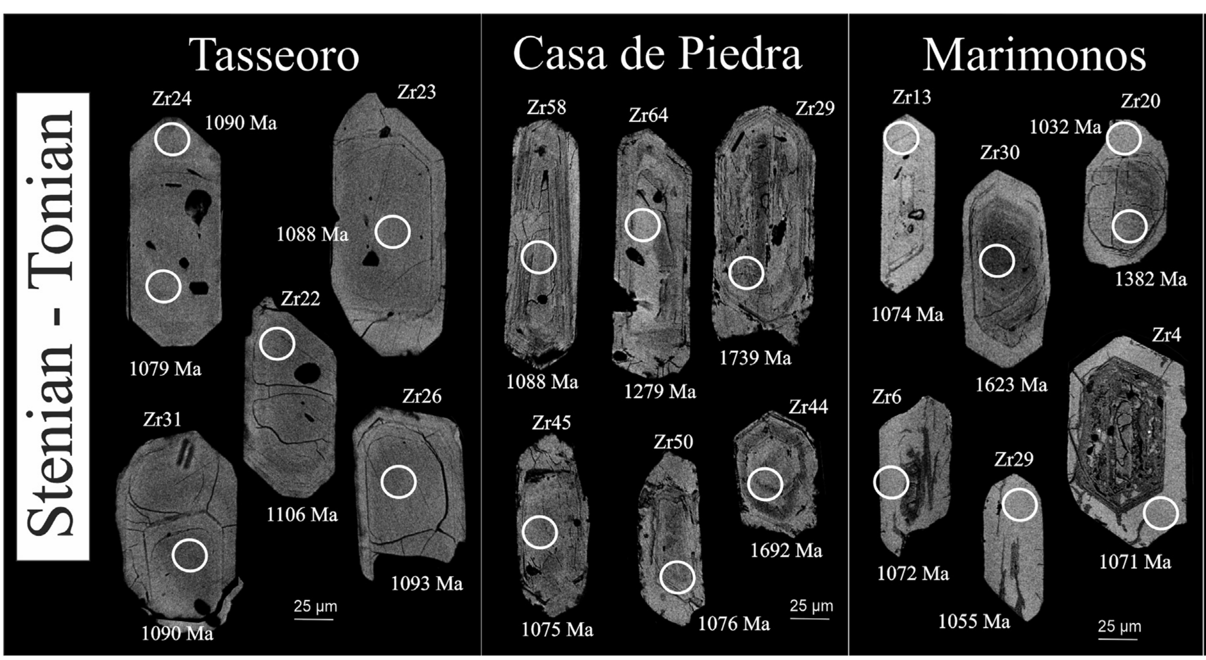

Fig. 9. Representative cathodoluminescence (CL) and backscattered electron (BSE) images for zircon grains from Stenian granitic plutons in the Sunsas belt. The Tasseoro intrusion sample presents zircon crystals with prismatic shapes, lengths between 100 and 300 μm and 2:1 length/width. BSE images show faint regular oscillatory zoning or unzoned crystals with many inclusions. The Casa de Piedra sample contains two morphological zircon groups. The most representative group is of prismatic elongated crystals, measuring 100–400 μm, ratio of 4:1. The other group is of rounded zircon crystals with subhedral shapes, lengths 100 to 300 μm, ratio 2:1; they show faint oscillatory zoning and zircon with homogeneous and xenocrystic cores truncated by growth of lighter rims. Zoning between core and rim is not well defined. Also, some crystals present dark cores, indicating high trace-element contents, and many inclusions of rounded and prismatic minerals. The Marimonos granitic pluton sample shows zircon grains with subhedral shapes, lengths of 120–350 μm, aspect ratio 2:1, and elongated prismatic crystals with lengths of 200–300 μm, aspect ratio 3:1, with complex internal structures. In general, crystals present homogeneous cores, oscillatory zoning and growth of unzoned rims with well delimited zoning between core and rim. Also, chaotically zoned cores in xenocrystic crystals with evidence for resorption and recrystallization are observed.

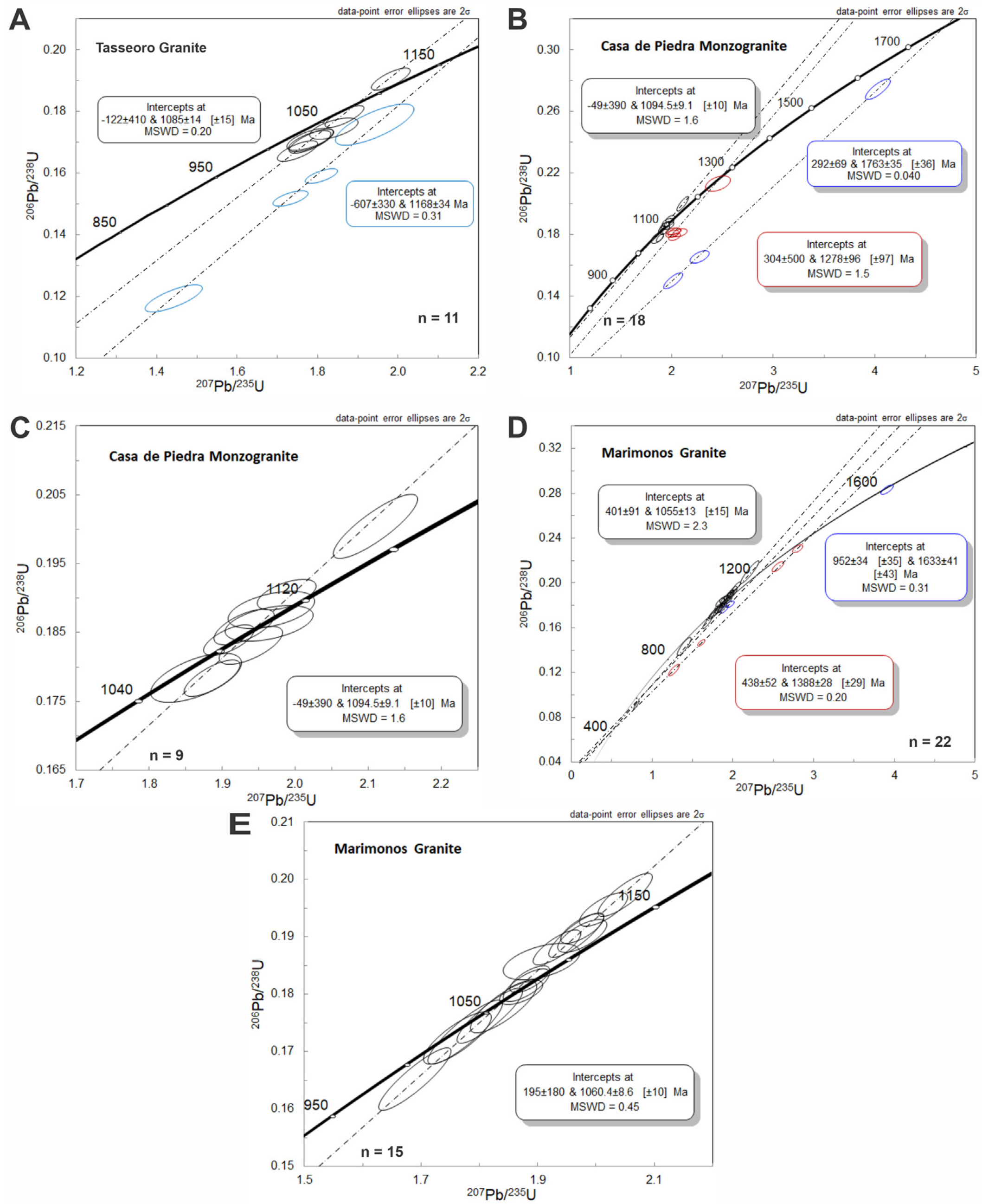

Fig. 10. U–Pb zircon diagrams for the (A) Tasseoro, (B–C) Casa de Piedra and (D–E) Marimonos granitic plutons from the Sunsas belt (Supplementary Data, Table S1).

one of the intra-oceanic magmatic arcs associated with the San Ignacio orogeny and recorded eastwards, in the Jauru Terrane (Santos et al., 2000; Matos et al., 2009; Bettencourt et al., 2010).

5.3. The Sunsas orogeny

The 1094 ± 9 Ma Casa de Piedra and 1055 ± 13 Ma Marimonos intrusions represent the youngest granite magmatism episodes in the northwestern domain of the Sunsas belt (Fig. 10; Table 1). Both granites are exposed between the NNW–SSE Blanco Ibiaimiai and Concepción shear zones, the regional structures that played such as magmatic channels (Fig. 3). In the southern domain, the Tasseoro granite was emplaced along the E–W San Diablo front and records two zircon crystallization ages at 1168 ± 34 Ma and 1085 ± 14 Ma, indicating a possible diachronic evolution for the magmatic activity along the front. This ~60–80 Ma age dispersion can represent a major magmatic pulse followed by a second pulse of Tasseoro final emplacement and solidification. On the other hand, the Th/U ratios > 0.1 (0.50–1.54) and the Tasseoro geographic position along the San Diablo front also may suggest that right after the pluton crystallization a tectono-thermal activity during the Sunsas orogenic peak opened the zircon system as recorded by the younger ages.

The 1.76 Ga, 1.62 Ga, and 1.38 Ga inherited zircon cores recorded in granitoids from the southern and northern Sunsas belt domains suggest crustal reworking of the 1.68 Ga Chiquitania and 1.81–1.65 Ga Lomas Maneches complexes (e.g., Paraguá Terrane) and of the Pensamiento Suite (e.g., San Ignacio orogeny).

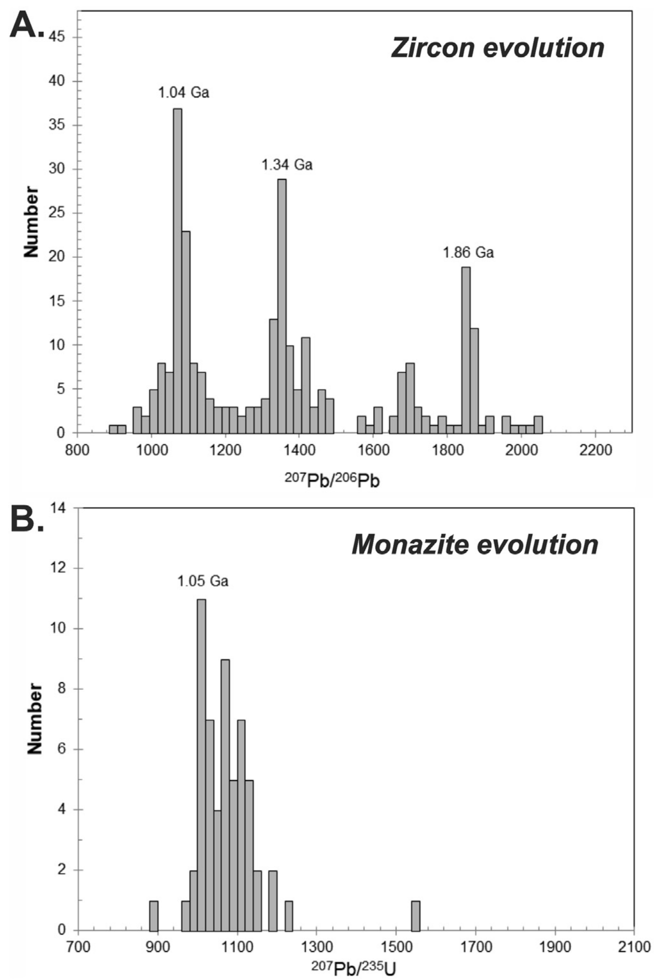

Fig. 11. (A) Histogram of ^{207}Pb/^{206}Pb zircon ages from the Sunsas belt. Compiled from Supplementary Data, Table S1, and Nedel et al. (2020); (B) histogram of ^{207}Pb/^{235}U monazite ages from the Sunsas belt. Data from Table 3.

5.4. U–Pb monazite ages

Monazite crystals contain considerable amounts of U (ppm) and mainly Th (wt.%) (e.g., Parrish, 1990; Rubatto et al., 2013). Radiogenic Pb is dominant in the monoclinic structure of monazite due to high closure temperature (>700 °C) for diffusive Pb loss, allowing younger ages to be measured (e.g., Parrish, 1990; Smith and Giletti, 1997). Therefore, monazite is the mineral of choice for timing magmatism, metamorphism, and establishing a timescale related to an orogenic event, particularly the timing of tectonic collision and post-collision heating (e.g., Vance and Harris, 1999; Rubatto et al., 2013).

In this study, monazite crystals from two granitic plutons were dated by the U–Pb method. The analyzed Las Tojas granite sample displays monazite grains included in K-feldspar and mica crystals. The monazite analyses yielded an upper intercept age of 992 ± 41 Ma in the Concordia diagram (Fig. 5A). The reversely discordant pattern of U–Pb analyses indicates excess of ^{206}Pb and commonly provides significantly younger ages than the mineral crystallization (Parrish, 1990). Therefore, the ^{207}Pb/^{235}U ages, that yielded a weighted mean of 1079 ± 14 Ma, indicate the best estimate for monazite crystallization. Thus, the monazite age matches the crystallization of the main zircon population from the Sunsas belt (Figs. 10 and 11; Table 1; Nedel et al., 2020), indicating that the monazite grains grew during a thermal peak of metamorphism related to the collisional stage of the Sunsas orogeny.

For the Señoritas granite, the monazite analyses yielded an upper intercept age of 1006 ± 8 Ma in the Concordia diagram (Fig. 5C). Different from the other analyses, they do not present a reverse discordance pattern. The ^{206}Pb/^{238}Pb monazite crystallization age (1006 ± 8 Ma) is coeval with Rb–Sr (1005 ± 12 Ma) and K–Ar (1008 ± 22 Ma to 935 ± 21 Ma) ages in biotite recorded in the Sunsas belt (Litherland et al., 1986). However, the weighted mean of ^{207}Pb/^{235}U ages of 1018 ± 6 Ma can provide a more precise estimate for monazite crystallization since there is no analytical Pb-loss influence. This age is in agreement with a thermal peak generated during the final collision of the Sunsas belt, whereas the post-tectonic to anorogenic stages took place after 1.0 Ga (Table 1; Teixeira et al., 2010).

Therefore, the 1079 ± 14 Ma and 1018 ± 6 Ma monazite crystallization ages imply monazite growth during a medium- to high-grade prograde metamorphic evolution of the Paleo- and Mesoproterozoic basement within the Sunsas belt during the Sunsas orogeny collisional phase (Fig. 11B, Table 3; Teixeira et al., 2010; Johnson et al., 2015; Nedel et al., 2020). Likewise, U–Pb monazite ages indicate that the 1.9 Ga and 1.4 Ga protolith sources were reworked during Rodinia assembly. Thus, the monazite results are relevant and can contribute to unravel a complex tectonic history for igneous rocks dated only by the U–Pb-in-zircon method (e.g., Rubatto et al., 2001; Piechocka et al., 2017).

5.5. Constraints for the SW Amazonian Craton

The geochronological results support a 1.9–1.8 Ga old felsic basement for the Sunsas belt southern domain, correlated to the Rio Apa Terrane (Figs. 2 and 11A). Therefore, this terrane possibly surpasses the limits previously established in the extreme south of the Sunsas belt extending southwards of the San Diablo front. In contrast, ~1.68 Ga old rocks represent the basement of the northern domain, related to the Chiquitania and Lomas Maneches complexes (Litherland et al., 1989; Teixeira et al., 2010).

Archean and Paleoproterozoic inherited zircon cores suggest a possible correlation between Paraguá Terrane protoliths and 2.2–1.8 Ga orogenies associated to the Nuna-Columbia assembly (Zhang et al., 2012; Teixeira et al., 2013; Faleiros et al., 2016; Nedel et al., 2020). However, these ages also may represent inheritance from sedimentary protoliths, which would not imply an older crustal link. The 1.87–1.85 Ga, 1.76–1.75 Ga, 1.35 Ga, and ~1.0 Ga magmatic episodes are recorded in northern Laurentia and support a long-lived connection among different blocks and terrains in the Proterozoic (e.g., Ernst et al., 2016). In this context, the Sunsas belt reveals a geochronological evolution similar to eastern Laurentia when it is taken into account that the Sunsas magmatism was generated between 1.1 Ga and 1.04 Ga, with a magmatic peak at 1.08 Ga, by the Paleoproterozoic and Mesoproterozoic protoliths reworking (e.g., Loewy et al., 2003; Spencer et al., 2015; Fig. 11A; Table 1).

The Sunsas belt displays 1.9–1.8 Ga felsic protoliths in the southern domain, whereas in the northwestern domain, the basement is formed of 1.7–1.6 Ga protoliths (Figs. 2 and 12). These Paleoproterozoic fragments were reworked and accreted to the Amazonian Craton during the 1.4–1.3 Ga San Ignacio orogeny (Fig. 12; Nedel et al., 2020). The 1.1–1.0 Ga Sunsas orogeny promoted a new partial melting of Paleo- and early Mesoproterozoic felsic crust. Our geochronological data confirm previous geodynamic correlations regarding Amazonia-Laurentia and Amazonia with the Rio Apa Terrane indicating that these crustal fragments may have shared the same evolution during Mesoproterozoic times (e.g., Boger et al., 2005; Fernandes et al., 2006; Tohver et al., 2006; Teixeira et al., 2010; Rizzotto et al., 2014; Nedel et al., 2020). Therefore, the crustal reworking of the distinct Paleoproterozoic basements during ~1.4–1.35 Ga and 1.1–1.0 Ga oroge-

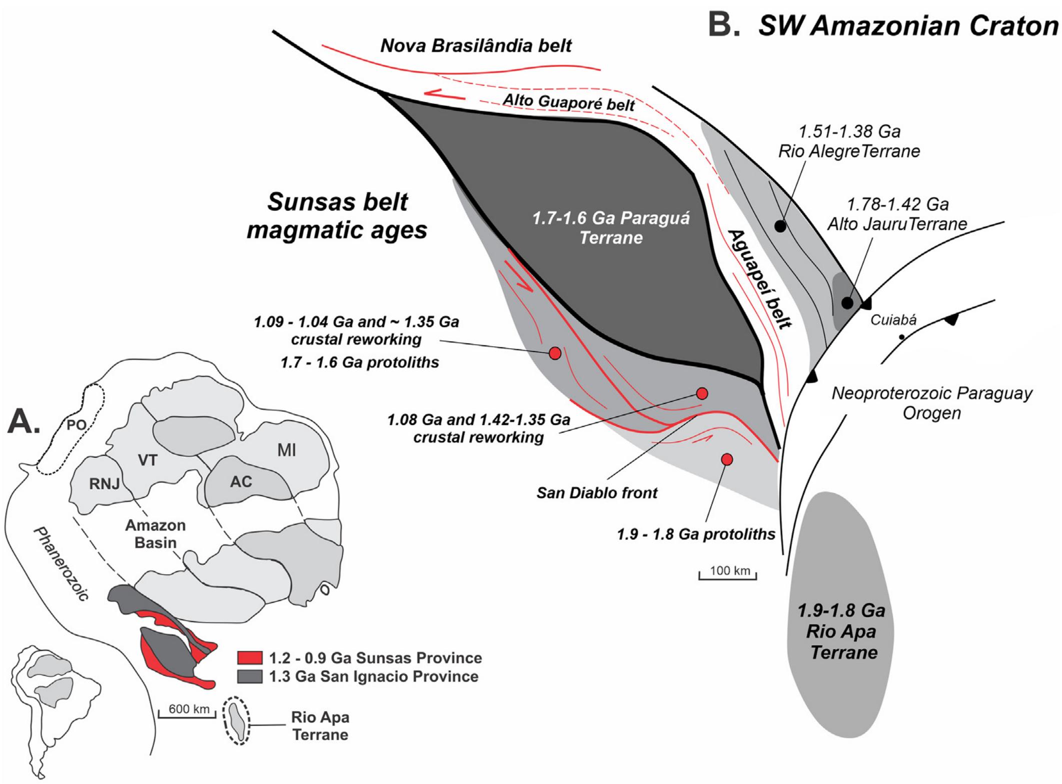

Fig. 12. (A) Schematic geotectonic compartmentation of the Amazonian Craton with emphasis on the SW portion; (B) schematic terrain distribution for the Sunsas Province, SW Amazonian Craton. Correlated ages of inherited zircon grains and protholith sources for the Sunsas belt magmatism.

nies were the major petrogenesis processes for the Sunsas belt assembly (Fig. 12).

6. Conclusion

Combined U–Pb zircon and monazite geochronological data reveal that the Sunsas belt was generated by several crustal reworking events from Paleoproterozoic sources. Specifically, the main contributions are:

(1) The Sunsas belt southern domain is formed of 1.9–1.8 Ga granitic magmatism correlated to the Rio Apa Terrane, whereas the northern domain encompasses 1.68 Ga magmatic rocks correlated to the Chiquitania and Lomas Maneches complexes of the Paraguá Terrane.
(2) 1.45 Ga and 1.42 Ga old granites reveal magmatic activity along the Sunsas belt related to the Santa Helena Orogen recorded in the Jauru Terrane.
(3) The 1.37–1.34 Ga granites from the Pensamiento Suite suggest a previous collision and reworking of the Paraguá Terrane during the San Ignacio orogeny.
(4) The Sunsas belt records significant granitic magmatism between 1.10 Ga and 1.05 Ga related to the last partial melting of the Paleoproterozoic sources.
(5) The 1079 ± 14 Ma and 1018 ± 6 Ma U–Pb monazite ages represent the prograde tectono-thermal event associated to the Sunsas orogeny collisional phase.

Declaration of Competing Interest

The authors declare that they have no known competing financial interests or personal relationships that could have appeared to influence the work reported in this paper.

Acknowledgements

The authors acknowledge the support of the Laboratório de Geocronologia (Universidade de Brasília) and the Grupo de Pesquisa em Evolução Crustal e Tectônica (Guaporé). This study was financed in part by the Coordenação de Aperfeiçoamento de Pessoal de Nível Superior - Brasil (CAPES) - Finance Code 001. The authors also acknowledge Fundação de Apoio à Pesquisa do Distrito Federal (FAPDF) and INCT Estudos Tectônicos (CNPq-CAPES-FAPDF) for financial support. IMN thanks CAPES and Programa de Excelência Acadêmica (PROEX, Edital - 0487) for granting the Doctorate scholarship. RAF and ASR acknowledge CNPq for research fellowship.

Appendix A. Supplementary data

Supplementary data to this article can be found online at https://doi.org/10.1016/j.gsf.2021.101247.

References

Albarède, F., Telouk, P., Blichert-Toft, J., Boyet, M., Agranier, A., Nelson, B., 2004. Precise and accurate isotopic measurements using multiple collector ICPMS. Geochim. Cosmochim. Acta 68, 2725–2744.
Aleinikoff, J.N., Schenk, W.S., Plank, M.O., Srogi, L.A., Fanning, C.M., Kamo, S.L., Bosbyshell, H., 2006. Deciphering igneous and metamorphic events in high-grade rocks of the Wilmington complex, Delaware: morphology, cathodoluminescence and backscattered electron zoning, and SHRIMP U-Pb geochronology of zircon and monazite. Geol. Soc. Am. Bull. 118, 39–64.
Araújo-Ruiz, L.M.B., 2003. Caracterização petrológica, geoquímica e geocronológica do Maciço Sararé (Nova Lacerda-MT). Masters Dissertation. Inst. de Geoc. e Ciências Exatas, Univers. Estadual Paulista-UNESP, Rio Claro (in Portuguese with English abstract).
Bettencourt, J.S., Leite Jr, W.B., Ruiz, A.S., Matos, R., Payolla, B.L., Tosdal, R.M., 2010. The Rondonian-San Ignacio Province in the SW Amazonian Craton: an overview. J. South Am. Earth Sci. 29, 28–46.

Bingen, B., Viola, G., Möller, C., Auwera, J.V., Laurent, A., Yi, K., 2021. The Sveconorwegian orogeny. Gondwana Res. 90, 273–313. https://doi.org/10.1016/j.gr.2020.10.014.
Boger, S.D., Raetz, M., Giles, D., Etchart, E., Fanning, C.M., 2005. U-Pb age from the Sunsás region of Eastern Bolivia, evidence for allochthonous origin of the Paraguá Block. Precambr. Res. 139, 121–146.
Brittes, A.F.N., Sousa, M.Z.A., Ruiz, A.S., Batata, M.E.F., Lafon, J.-M., Plens, D.P., 2013. Geology, petrology and geochronology (Pb-Pb) of the Serra da Bocaina Formation: evidence of an Orosirian Amoguijá Magmatic Arc in the Rio Apa Terrane, south of the Amazonian Craton. Braz. J. Geol. 43, 48–69.
Bühn, B.M., Pimentel, M.M., Matteini, M., Dantas, E.L., 2009. High spatial resolution analyses of Pb and U isotopes for geochronology by laser ablation multi-collector inductively coupled plasma mass spectrometry LA-MC-ICP-MS. An. Acad. Bras. Ciênc. 81, 1–16.
Cawood, P.A., Hawkesworth, C.J., Dhuime, B., 2013. The continental record and the generation of continental crust. Geol. Soc. Am. Bull. 125, 14–32.
Chaves, M.L.S.C., Brandão, P.R.G., Buhn, B., 2010. Monazita em veios de quartzo da Serra do Espinhaço Meridional (MG): mineralogia, idades LA-ICP-MS e implicações geológicas. Rev. Bras. Geoc. 40, 506–515 (in Portuguese with English abstract).
Condie, K.C., 2004. Supercontinents and superplume events: distinguishing signals in the geologic record. Phys. Earth Planet. Inter. 146, 319–332.
Cordani, U.G., Teixeira, W., 2007. Proterozoic accretionary belts in the Amazonian Craton. Geol. Soc. Am. Bull. Memoir 200, 297–320.
Cordani, U.G., Sato, K., Teixeira, W., Tassinari, C.C.G., and Basei, M.A.S., 2000. Crustal evolution of the South American platform. In: Cordani, U.G., Milani, E.J., Thomaz-Filho, A., Campos, D.A. (Eds.), Tectonic evolution of South America: Rio de Janeiro, Brazil, 31st International Geological Congress, 19–40.
Cordani, U.G., Teixeira, W., Tassinari, C.C.G., Coutinho, J.M.V., Ruiz, A.S., 2010. The Rio Apa Craton in Mato Grosso do Sul (Brazil) and northern Paraguay: Geochronological evolution, correlations and tectonic implications for Rodinia and Gondwana. Gondwana Res. 15, 396–407.
Corfu, F., Hanchar, J.M., Hoskin, P.W.O., Kinny, P., 2003. Atlas of zircon textures. Rev. Mineral. Geochem. 53, 469–500.
Darbyshire, D.P.F., 2000. The Precambrian of Eastern Bolívia−Sm-Nd isotope study. The 31st Int. Geol. Congress, Rio de Janeiro, Brazil, Abstr. Vol. Rio de Janeiro, Geol. Surv. Brazil.
Ernst, R.E., Hamilton, M.A., Söderlund, U., Hanes, J.A., Gladkochub, D.P., Okrugin, A. V., Kolotolina, T., Mekhonoshin, A.S., Bleeker, W., Cheminant, A.N., Buchan, K.L., Chamberlain, K.R., Didenko, A.N., 2016. Long-lived connection between southern Siberia and northern Laurentia in the Proterozoic. Nat. Geosci. 9, 464–469.
Faleiros, F.M., Pavan, M., Remédio, M.J., Rodrigues, J.B., Almeida, V.V., Caltabeloti, F. P., Pinto, L.G.R., Oliveira, A.A., Pinto de Azevedo, E.J., Costa, V.S., 2016. Zircon U-Pb ages of rocks from the Rio Apa cratonic Terrane (Mato Grosso do Sul, Brazil): new insights for its connection with the Amazonian Craton in pre-Gondwana times. Gondwana Res. 34, 187–204.
Fernandes, C.J., Kuyumjian, R.M., Pulz, G.M., Geraldes, M.C., Pinho, F.E.C., 2006. Geologia estrutural e idade 40Ar/39Ar do depósito de ouro Pau-a-Pique, Faixa Móvel Aguapeí, sudoeste do Estado do Mato Grosso. Rev. Bras. Geoc. 36, 3–15 (in Portuguese with English abstract).
Ferreira, A.C.D., Dantas, E.L., Fuck, R.A., Nedel, I.M., 2020. Arc accretion and crustal reworking from late Archean to Neoproterozoic in Northeast Brazil. Sci. Rep. 10, 7855.
Fioretti, A.M., Black, L.P., Foden, J., Visona, D., 2005. Grenville-age magmatism at the South Tasman Rise (Australia): a new piercing point for the reconstruction of Rodinia. Geology 33, 769–772.
Fitzsimons, I.C.W., 2000. Grenville-age basement provinces in East Antarctica: evidence for three separates collisional orogens. Geology 28, 879–882.
Fuck, R.A., Brito Neves, B.B., Schobbenhaus, C., 2008. Rodinia descendants in South America. Precambr. Res. 160, 108–126.
Geraldes, M.C., 2000. Geocronologia e geoquímica do plutonismo Mesoproterozoico do SW do Estado de Mato Grosso (SW do Cráton Amazônico). Ph.D. thesis, São Paulo. Inst. de Geoc. Universidade de São Paulo (in Portuguese with English abstract).
Geraldes, M.C., Van Schmus, W.R., Condie, K.C., Bell, S., Teixeira, W., Babinski, M., 2001. Proterozoic geologic evolution of the SW part of the Amazonian Craton in Mato Grosso state, Brazil. Precambr. Res. 111, 91–128.
Hawkesworth, C.J., Dhuime, B., Pietranik, A.B., Cawood, P.A., Kemp, A.I.S., Storey, C. D., 2010. The generation and evolution of the continental crust. J. Geol. Soc., London 167, 229–248.
Hodych, J.P., Cox, R.A., Košler, J., 2004. An equatorial Laurentia at 550 Ma confirmed by Grenvillian inherited zircons dated by LAM ICP-MS in the Skinner Cove volcanics of western Newfoundland: implications for inertial interchange true polar wander. Precambr. Res. 129, 93–113.
Hoffman, P.F., 1991. Did the breakout of Laurentia turn Gondwanaland inside-out?. Science 252, 1409–1412.
Holder, R.M., Viete, D.R., Brown, M., Johnson, T.E., 2019. Metamorphism and the evolution of plate tectonics. Nature 572, 378–381.
Ibañez–Mejia, M., 2020. The Putumayo Orogen of Amazonia: A synthesis. In: Gómez, J., Mateus–Zabala, D. (Eds.), The Geology of Colombia, Volume 1 Proterozoic – Paleozoic. Serv. Geol. Colombiano, Publicaciones Geológicas Especiales, Bogotá, 35, 101–131. https://doi.org/10.32685/pub.esp.35.2019.06.
Ibañez-Mejia, M., Ruiz, J., Valencia, V.A., Cardona, A., Gehrels, G.E., Mora, A.R., 2011. The Putumayo Orogen of Amazonia and its implications for Rodinia reconstructions: New U-Pb geochronological insights into the Proterozoic tectonic evolution of northwestern South America. Precambr. Res. 191 (1–2), 58–77. https://doi.org/10.1016/j.precamres.2011.09.005.
Isla-Moreno, L., 2009. Distrito Don Mario, un deposito de Au-Cu hidrotermal asociado a zonas de cizalla. XVIII Cong. Geol. Bolivia, Potosi. Memorias del Colegio de Geólogos, 85–92 (in Spanish).
Jackson, S.E., Pearson, N.J., Griffin, W.L., Belousova, E.A., 2004. The application of laser ablation-inductively coupled plasma-mass spectrometry to in situ U-Pb zircon geochronology. Chem. Geol. 211, 47–69.
Johnson, T.E., Clark, C., Taylor, R.J.M., Santosh, M., Collins, A.S., 2015. Prograde and retrograde growth of monazite in migmatites: an example from the Nagercoil Block, southern India. Geosci. Front. 6, 373–87.
Keppie, J.D., Dostal, J., Cameron, K.L., Solari, L.A., Ortega-Gutierrez, F., Lopez, R., 2003. Geochronology and geochemistry of Grenvillian igneous suites in the northern Oaxacan Complex, southern Mexico: tectonic implications. Precambr. Res. 120, 365–389.
Lacerda-Filho, J.V., Brito, R.S.C., Silva, M.G., Oliveira, C.C. De., Moreton, L.C., Martins, E.G., Lopes, R.C., Lima, T.M., Larizzatti, J.H., Valente, C.R., 2006. Geologia e Recursos Minerais do Estado de Mato Grosso do Sul. Programa integração, atualização e difusão de dados de geologia do Brasil. Convênio CPRM/SICME - MS, MME. 10 - 28 (in Portuguese).
Lacerda-Filho, J.V., Fuck, R.A., Ruiz, A.S., Dantas, E.L., Scandolara, J.E., Rodrigues, J.B., Nascimento, N.D.C., 2016. Palaeoproterozoic tectonic evolution of the Alto Tererê Group, southernmost Amazonian Craton, based on field mapping, zircon dating and rock geochemistry. J. South Am. Earth Sci. 65, 122–141.
Lacerda-Filho, J.V., Fuck, R.A., Ruiz, A.S., Dantas, E.L., Rodrigues, J.B., Scandolara, J.E., 2020. Rio Apa Block: A juvenile crustal fragment in SW Amazonian Craton and its implications for Columbia supercontinent reconstitution. J. Geol. 128 (5), 415–444.
Li, Z.X., Li, X., Zhou, H., Kinny, P.D., 2002. Grenvillian continental collision in South China: new SHRIMP U-Pb zircon results and implications for the configuration of Rodinia. Geology 30, 163–166.
Li, Z.X., Bogdanova, S.V., Collins, A.S., Davidson, A., De Waele, B., Ernst, R.E., Fitzsimons, I.C.W., Fuck, R.A., Gladkochub, D.P., Jacobs, J., Karlstrom, K.E., Lu, S., Natapov, L.M., Pease, V., Pisarevsky, S.A., Thrane, K., Vernikovsky, V., 2008. Assembly, configuration and break-up history of Rodinia: A synthesis. Precambr. Res. 1–2, 179–210.
Litherland, M., Bloomfield, K., 1981. The Proterozoic history of eastern Bolivia. Precambr. Res. 15, 157–179.
Litherland, M., Annells, R.N., Appleton, J.D., Berrange, J.P., Bloomfield, K., Burton, C.C. I., Darbyshire, D.P.F., Fletcher, C.J.N., Hawkins, M.P., Klinck, B.A., Llanos, A., Mitchell, W.I., O'Connor, E.A., Pitfield, P.E.J., Power, G., Webb, B.C., 1986. The Geology and Mineral Resources of the Bolivian Precambrian Shield. British Geological Survey, Overseas Memoir 9, 153.
Litherland, M., Annels, R.N., Hawkins, M.P., Klinck, B.A., O'Connor, E.A., Pitfield, P.E.J., Power, G., Darbyshire, D.P.F., Fletcher, C.N.J., Mitchell, W.I., Webb, B.C., 1989. The Proterozoic of eastern Bolivia and its relationships to the Andean mobile belt. Precambr. Res. 43, 157–174.
Loewy, S., Connelly, J.N., Dalziel, I.W., Gower, C.F., 2003. Eastern Laurentia in Rodinia: Constraints from whole-rock Pb and U-Pb geochronology. In: Sircombe, K.N., McElhinny, M.W. (Eds.), Orogenic belts, regional and global tectonics: A memorial volume to Chris McAulay Powell. Tectonophys 375, 169–197.
Loewy, S.L., Connelly, J.N., Dalziel, I.W.D., 2004. An orphaned basement block: the Arequipa-Antofalla Basement of the central Andean margin of South America. Geol. Soc. Am. Bull. 116, 171–187.
Ludwig, K.R., 2003. User's manual for Isoplot/Ex version 3.00, a geochronological toolkit for Microsoft Excel. Berkeley Geochronology Center Special Publications 4, 72pp.
Ludwig, K.R., 2008. User's Manual for Isoplot 3.70. A geochronological Toolkit for Microsoft Excel. Berkeley Geochronology Center 4(4), 76.
Manzano, J.C., Godoy, A.M., Araujo, L.M.B., Godoy, L.P., 2012. Suite plutônica Alumiador, Grupo Amoguijá, Maciço Rio Apa – MS. Geociências 31, 351–370 (in Portuguese).
Matos, R., Teixeira, W., Geraldes, M.C., Bettencourt, J.S., 2009. Geochemistry and Nd–Sr isotopic signatures of the Pensamiento Granitoid Complex, Rondonian-San Ignacio Province, Eastern Precambrian Shield of Bolivia: Petrogenetic constraints for a Mesoproterozoic magmatic arc settting. Geol. USP, Sér. Cient. 9, 89–117.
McLelland, J., Daly, J.S., McLelland, J.M., 1996. The Grenville orogenic cycle (ca. 1350–1000 Ma): An Adirondack perspective. Tectonophys 265, 1–28.
Meert, J.G., 2001. Growing Gondwana and refining Rodinia: a paleomagnetic perspective. Gondwana Res. 4, 279–288.
Menezes, R.G., Silva, P.C.S., Silva, L.C., Takahashi, A.T., Lopes Junior, I., Bezerra, J.R.I., 1993. Folha SD.21-Y-C-II. Pontes e Lacerda. Brasília: Ministério das Minas e Energia, Departamento Nacional da Produção Mineral, Projeto Levantamentos Geológicos Básicos do Brasil, Relatório Final, 126 (in Portuguese).
Nance, D.R., Murphy, B.J., Santosh, M., 2014. The supercontinent cycle: A retrospective essay. Gondwana Res. 25, 4–29.
Nedel, I.M., Ruiz, A.S., Matos-Salinas, G.R., Sousa, M.Z.A., Pimentel, M.M., Pavanetto, P., 2017. Front San Diablo na região de Miraflores, Faixa Sunsás, Bolívia: implicações tectônicas e estratigráficas. Geol. USP, Sér. Cient. 17, 12-147 (in Portuguese with English abstract).
Nedel, I.M., Fuck, R.A., Ruiz, A.S., Matos-Salinas, G.R., Ferreira, A.C.D., 2020. U-Pb geochronology and geochemistry of Grenville-age plutons in the Sunsás Belt - Bolivia, SW Amazonian Craton: Tectonic and magmatic implications. J. South Am. Earth Sci. 104, 102845. https://doi.org/10.1016/j.jsames.2020.102845.

Oliveira, F.V., 2015. Chronus: Um novo suplemento para a redução de dados U-Pb obtidos por LAMC-ICPMS. Geoc. Dissertation, Universidade de Brasília, Inst. Geoc. 348 (in Portuguese with English abstract).

Parrish, R.R., 1990. U-Pb dating of monazite and its application to geological problems. Can. J. Earth Sci. 27, 1431–1450.

Piechocka, A.M., Gregory, C.J., Zi, J.W., Sheppard, S., Wingate, M.T.D., Rasmussen, B., 2017. Monazite trumps zircon: applying SHRIMP U-Pb geochronology to systematically evaluate emplacement ages of leucocratic, low-temperature granites in a complex Precambrian orogen. Contrib. Miner. Petrol. 172, 63.

Plens, D.P., 2018. Petrogênese e análise estrutural da Suíte Caracol: implicações para a evolução geodinâmica do Bloco Rio Apa, sul do Cráton Amazônico. Doctoral Thesis. Universidade de Brasília, 117 (in Portuguese with English abstract).

Plens, D.P., Ruiz, A.S., Sousa, M.Z.A., Batata, E.F., Lafon, J.M., Brittes, A.F.N., 2013. Cerro Porã Batholith: post-orogenic A-type granite from the Amoguijá Magmatic Arc – Rio Apa Terrane – South of the Amazonian Craton. Braz. J. Geol. 43 (3), 515–534.

Quadros, M.L., Della Giustina, M.E., Souza, V.S., Scandolara, J.E., 2020. Geology, geochemistry and Sr-Nd isotopes of the Rio Branco Suite, Nova Brasilândia belt in southwest of the Amazonian Craton: Evidence of a Rodinia pre-assembly accretionary phase (ca. 1137 and 1106 Ma) during the evolution of the Nova Brasilândia orogeny. Lithos, 105651. https://doi.org/10.1016/j.lithos.2020.105651.

Redes, L.A., Pimentel, M.M., Ruiz, A.S., Matos, G.R.S., 2016. Granito Correreca - um registro magmático o no oriente boliviano: implicações tectônicas e estratigráficas. In: Anais do 48 Congresso Brasileiro de Geologia – Porto Alegre – Brazil (in Portuguese).

Redes, L.A., Pimentel, M.M., Ruiz, A.S., Matos, G.R.S., Nedel, I.M., 2018. Granito Santa Terezita – Magmatismo do Bloco Rio Apa a Sul do Aulacógeno Tucavaca - Oriente Boliviano. In: Anais do 49 Congresso Brasileiro de Geologia – Rio de Janeiro – Brazil (in Portuguese).

Redes, L.A., Hauser, N., Ruiz, A.S., Matos, R.S., Reimold, W.U., Dantas, E.L., Schmitt, R. T., Lima, B.A.F., Zacchi, E.N.P., Chaves, J.G.S., Osorio, L.F.B., Pimentel, M.M., 2020. U-Pb and Hf Isotopes in Granitoids from the eastern Bolivian Basement: insights into the Paleoproterozoic evolution of the western part of South America. J. South Am. Earth Sci. 104,. https://doi.org/10.1016/j.jsames.2020.102806 102806.

Rizzotto, G.J., 1999. Petrologia e Ambiente Tectônico do Grupo Nova Brasilândia-RO. Dissertação de Mestrado, Universidade Federal do Rio Grande do Sul, Porto Alegre, 136 p (in Portuguese with English abstract).

Rizzotto, G.J., Hartmann, L.A., Santos, J.O.S., McNaughton, N.J., 2014. Tectonic evolution of the southern margin of the Amazonian craton in the late Mesoproterozoic based on field relationships and zircon U-Pb geochronology. An. Acad. Bras. Ciênc. 86, 57–84.

Rubatto, D., Williams, I.S., Buick, I.S., 2001. Zircon and monazite response to prograde metamorphism in the Reynolds Range, central Australia. Contrib. Miner. Petrol. 140 (4), 458–468. https://doi.org/10.1007/pl00007673.

Rubatto, D., Chakraborty, S., Dasgupta, S., 2013. Timescales of crustal melting in the Higher Himalayan Crystallines (Sikkim, Eastern Himalaya) inferred from trace element-constrained monazite and zircon chronology. Contrib. Miner. Petrol. 165, 349–372.

Ruiz, A.S., 2005. Evolução geológica do sudoeste do Cráton Amazônico região limítrofe Brasil-Bolívia – Mato Grosso. Doctoral Thesis. Inst. de Geoc. e Ciências Exatas. Universidade Estadual Júlio de Mesquita Filho, Rio Claro (in Portuguese with English abstract).

Sadowski, G.R., Bettencourt, J.S., 1996. Mesoproterozoic tectonic correlations between eastern Laurentia and the western border of the Amazon Craton. Precambr. Res. 76, 213–227.

Saes, G.S., Leite, J.A.D., 1993. Evolução tectono-sedimentar do Grupo Aguapeí, Proterozóico Medio na porção meridional do Craton Amazonico: Mato Grosso e oriente boliviano. Rev. Bras. Geoc. 23, 31–38 (in Portuguese with English abstract).

Santos, J.O.S., Hartmann, L.A., Gaudette, H.E., Groves, D.I., McNaughton, N.J., Fletcher, I.R., 2000. A new understanding of the Amazon Craton provinces based on integration of field mapping and U-Pb and Sm-Nd geochronology. Gondwana Res. 3, 453–488.

Santos, J.O.S., Rizzotto, G.J., Potter, P.E., McNaughton, N.J., Matos, R.S., Hartmann, L. A., Chemale Jr., F., Quadros, M.S., 2008. Age and autochthonous evolution of the Sunsás Orogen in West Amazon Craton based on mapping and U-Pb geochronology. Precambr. Res. 165, 120–152.

Schärer, U., 1984. The effect of initial ^{230}Th disequilibrium on young U-Pb ages: the Makalu case, Himalaya. Earth Planet. Sci. Lett. 67, 191–204.

Siqueira, L.H., 2015. Granito São Domingos: Registro de Magmatismo Pós-Tectônico do Orógeno Intracontinental Aguapeí, SW do Cráton Amazônico. Universidade Federal de Mato Grosso. Masters Dissertation. Inst. de Ciênc. Exatas e da Terra. Dep. de Recursos Minerais (in Portuguese with English abstract).

Smith, H.A., Giletti, B.J., 1997. Pb diffusion in monazite. Geochim. Cosmochim. Acta 51, 1047–1055.

Spencer, C.J., Cawood, P.A., Hawkesworth, C.J., Prave, A.R., Robets, N.M.W., Horstwood, M.S.A., Whitehouse, M.J., EIMF, 2015. Generation and preservation of continental crust in the Grenville Orogeny. Geosci. Front. 6(3), 357-372. https://doi:10.1016/j.gsf.2014.12.001.

Tassinari, C.C.G., Macambira, M.J.B., 1999. Geochronological provinces of the Amazonian Craton. Episodes 38, 174–182.

Tassinari, C.C.G., Macambira, M.J.B., 2004. A evolução tectônica do Cráton Amazônico. In: Mantesso-Neto, V., Bartorelli, A., Carneiro, C.R., Brito-Neves, B. B. (Eds.), Geologia do Continente Sul-Americano. São Paulo, Beca, pp. 471–485 (in Portuguese).

Tassinari, C.C.G., Bettencourt, J.S., Geraldes, M.C., Macambira, M.J.B., Lafon, J.M., 2000. The Amazonian Craton. In: Cordani, U.G., Miliani, E.J., Thomaz-Filho, A., Campos, D.A. (Eds.), Tectonic Evolution of South America. 31st International Geological Congress, Rio de Janeiro, Brazil, pp. 41–95.

Teixeira, W., Tassinari, C.C.G., Cordani, U.G., Kawashita, K., 1989. A review of the geochronology of the Amazonian Craton: tectonic implications. Precambr. Res. 42, 213–227.

Teixeira, W., Geraldes, M.C., Matos, R., Ruiz, A.S., Saes, G., Vargas-Mattos, G., 2010. A review of the tectonic evolution of the Sunsás belt, SW Amazonian Craton. J. South Am. Earth Sci. 29, 47–60.

Teixeira, W., D'Agrella-Filho, M.S., Hamilton, M.A., Ernst, R.E., Girardi, V.A.V., Mazzucchelli, M., Bettencourt, J.S., 2013. U-Pb (ID-TIMS) baddeleyite ages and paleomagnetism of 1.79 and 1.59 Ga tholeiitic dyke swarms, and position of the Rio de la Plata Craton within the Columbia supercontinent. Lithos 174, 157–174.

Teixeira, W., Hamilton, M.A., Lima, G.A., Ruiz, A.S., Matos, R., Ernst, R.E., 2015. Precise ID-TIMS U-Pb baddeleyite ages (1110–1112 Ma) for the Rincón del Tigre-Huanchaca large igneous province (LIP) of the Amazonian Craton: Implications for the Rodinia supercontinent. Precambr. Res. 265, 273–285.

Teixeira, W., Cordani, U.G., Faleiros, F.M., Sato, K., Maurer, V.C., Ruiz, A.S., Azevedo, E. J.P., 2020. The Rio Apa Terrane reviewed: U-Pb zircon geochronology and provenance studies provide paleotectonic links with a growing Proterozoic Amazonia. Earth Sci. Rev. 202,. https://doi.org/10.1016/j.earscirev.2020.103089 103089.

Tohver, E., Van der Pluijm, B.A., Van der Voo, R., Rizzotto, G.J., Scandolara, J.E., 2002. Paleogeography of the Amazon Craton at 1.2 Ga: early Grenvillian collision with the Llano segment of Laurentia. Earth Planet. Sci. Lett. 199, 185–200.

Tohver, E., Bettencourt, J.S., Tosdal, R., Mezger, K., Leite, W.B., Payolla, B.L., 2004. Terrane transfer during the Grenville orogeny: tracing the Amazonian ancestry of southern Appalachian basement through Pb and Nd isotopes. Earth Planet. Sci. Lett. 228, 161–176.

Tohver, E., Teixeira, W., Van der Pluijm, B.A., Geraldes, M.C., Bettencourt, J.S., Rizzotto, G., 2006. A restored transect across the exhumed Grenville orogen of Laurentia and Amazonia, with implications for crustal architecture. Geology 34, 669–672.

Vance, D., Harris, N., 1999. The timing of prograde metamorphism in the Zanskar Himalaya. Geology 27, 395–398.

Vargas-Mattos, G.L., 2010. Caracterização geocronológica e geoquímica dos granitos proterozoicos: implicação para a evolução crustal da borda SW do Cráton Amazônico na Bolívia. Doctoral Thesis. Faculdade de Geologia, Universidade do Estado do Rio de Janeiro, 164 p (in Portuguese with English abstract).

Wiedenbeck, M., Hanchar, J.M., Peck, W.H., Sylvester, P., Valley, J., Whitehouse, M., Kronz, A., Morishita, Y., Nasdala, L., Fiebig, J., Franchi, I., Girard, J.P., Greenwood, R.C., Hinton, R., Kita, N., Mason, P.R.D., Norman, M., Ogasawara, M., Piccoli, P.M., Rhede, D., Satoh, H., Schulz-Dobrick, B., Skår, O., Spicuzza, M.J., Terada, K., Tindle, A., Togashi, S., Vennemann, T., Xie, Q., Zheng, Y.F., 2004. Further characterisation of the 91500-zircon crystal. Geostand. Geoanal. Res. 28, 9–39. https://doi.org/10.1111/j.1751-908X.2004.tb01041.x.

Williams, M.L., Jercinovic, M.J., Hetherington, C.J., 2007. Microprobe monazite geochronology: Understanding geologic processes by integrating composition and chronology. Annu. Rev. Earth Planet. Sci. 35 (1), 137–175. https://doi.org/10.1146/annurev.earth.35.031306.140228.

Zhang, S., Li, Z.-X., Evans, D.A.D., Wu, H., Li, H., Dong, J., 2012. Pre-Rodinia supercontinent Nuna shaping up: a global synthesis with new paleomagnetic results from North China. Earth Planet. Sci. Lett. 353–354, 145–155.